AD-A266 890

ARMY RESEARCH LABORATORY

Static Aeroelastic Response of an Aircraft With Asymmetric Wing Planforms Representative of Combat Damage

Jong-Ho Woo

ARL-TR-153 June 1993

NOTICES

REPORT DOCUMENTATION PAGE

Form Approved
OMB No. 0704-0188

1. AGENCY USE ONLY (*Leave blank*)

2. REPORT DATE
June 1993

3. REPORT TYPE AND DATES COVERED
Final, Oct 91-Oct 92

4. TITLE AND SUBTITLE
Static Aeroelastic Response of an Aircraft With Asymmetric Wing Planforms Representative of Combat Damage

5. FUNDING NUMBERS
PR: 1L162618AH80

6. AUTHOR(S)
Jong-Ho Woo

7. PERFORMING ORGANIZATION NAME(S) AND ADDRESS(ES)
U.S. Army Research Laboratory
ATTN: AMSRL-SL-BA
Aberdeen Proving Ground, MD 21005-5068

8. PERFORMING ORGANIZATION REPORT NUMBER

9. SPONSORING/MONITORING AGENCY NAME(S) AND ADDRESS(ES)
U.S. Army Research Laboratory
ATTN: AMSRL-OP-CI-B (Tech Lib)
Aberdeen Proving Ground, MD 21005-5066

10. SPONSORING/MONITORING AGENCY REPORT NUMBER
ARL-TR-153

11. SUPPLEMENTARY NOTES

12a. DISTRIBUTION/AVAILABILITY STATEMENT
Approved for public release; distribution is unlimited.

12b. DISTRIBUTION CODE

13. ABSTRACT (*Maximum 200 words*)

This report describes an analysis of the static aeroelastic response of an aircraft with asymmetrical wing planforms representing combat damage. The analysis was performed using the MSC/NASTRAN Aeroelastic Code. Structural and aerodynamic models are based on the finite element approach and are created independently for both the damaged and undamaged cases. Fuselage, wings (with aileron), stabilators, and vertical wings (with rudders) are considered as lifting and control surfaces in the aerodynamic model. Five different wing structural models, one undamaged and four damaged, are examined in this report. Doublet-Lattice subsonic theory is used to account for interference effects among multiple lifting surfaces and bodies. The stability and control derivatives, airloads, and trim values are obtained for the damaged-wing aircraft. Effects of damage, including the influence of wing-body interference, on the aircraft's flight dynamics are discussed.

14. SUBJECT TERMS
T-38 aircraft; aerodynamic model, control and stability derivatives; MSC/NASTRAN; aeroelasticity, damage wing, control surfaces

15. NUMBER OF PAGES
62

16. PRICE CODE

17. SECURITY CLASSIFICATION OF REPORT	18. SECURITY CLASSIFICATION OF THIS PAGE	19. SECURITY CLASSIFICATION OF ABSTRACT	20. LIMITATION OF ABSTRACT
UNCLASSIFIED	UNCLASSIFIED	UNCLASSIFIED	UL

INTENTIONALLY LEFT BLANK

TABLE OF CONTENTS

LIST OF FIGURES

LIST OF TABLES

INTENTIONALLY LEFT BLANK

ACKNOWLEDGMENTS

The author wishes to express gratitude to Dr. Donald F. Haskell, former Chief of the Air Systems Branch, US Army Research Laboratory, Aberdeen Proving Ground, MD, for his technical and administrative support of this project. The author would also like to thank the Macneal-Schwendler Corporation for their technical support.

INTENTIONALLY LEFT BLANK

NOMENCLATURE

C	Reference chord, in
C_L	Lift moment coefficient
C_l	Rolling moment coefficient
C_{l_p}	Damping-in-roll derivative
C_{l_q}	Rolling moment coefficient derivative due to pitching
C_{l_r}	Rolling moment coefficient derivative due to yawing
C_{l_α}	Rolling moment coefficient derivative due to angle of attack
C_{l_β}	Dihedral effect
$C_{l_{\delta_a}}$	Rolling moment coefficient derivative due to aileron deflection
$C_{l_{\delta_s}}$	Rolling moment coefficient derivative due to stabilator deflection
$C_{l_{\delta_r}}$	Rolling moment coefficient derivative due to rudder deflection
C_m	Pitching moment coefficient
C_{m_α}	Pitching moment curve slope
$C_{m_{\dot\alpha}}$	Angle of attack damping coefficient
C_{m_p}	Pitching moment coefficient derivative due to rolling
C_{m_q}	Pitch damping coefficient derivative
$C_{m_{\delta_a}}$	Pitching moment coefficient derivative due to aileron deflection
$C_{m_{\delta_s}}$	Pitching moment coefficient derivative due to stabilator deflection
C_n	Yawing moment coefficient
C_{n_p}	Yawing moment coefficient derivative due to rolling
C_{n_q}	Yawing moment coefficient derivative due to pitching
C_{n_r}	Damping-in-yaw derivative
C_{n_α}	Yawing moment coefficient derivative due to angle of attack
C_{n_β}	Weathercock stability derivative
$C_{n_{\delta_a}}$	Yawing moment coefficient derivative due to aileron deflection

$C_{n_{\delta_s}}$	Yawing moment coefficient derivative due to stabilator deflection
$C_{n_{\delta_r}}$	Yawing moment coefficient derivative due to rudder deflection
C_x	Axial force coefficient
C_y	Side force coefficient
C_{y_p}	Side force due to rolling
C_{y_r}	Side force due to yawing
C_{y_β}	Side force coefficient derivative act in the y-direction
$C_{y_{\delta_a}}$	Side force coefficient derivative due to aileron deflection
$C_{y_{\delta_r}}$	Side force coefficient derivative due to rudder deflection
C_z	Normal force coefficient
C_{z_o}	Normal force coefficient at zero incidence and control deflection
C_{z_q}	Normal force due to pitching
C_{z_α}	Lift curve slope
$C_{z_{\delta_a}}$	Normal force coefficient derivative due to aileron deflection
$C_{z_{\delta_s}}$	Normal force coefficient derivative due to stabilator deflection
I_{xx}	Moment of inertia about x-axis, lb-in^2
I_{yy}	Moment of inertia about y-axis, lb-in^2
I_{zz}	Moment of inertia about z-axis, lb-in^2
V	Aircraft speed, ft/sec
L_f	Fuselage length, in
X	Roll axis
Y	Pitch axis
Z	Yaw axis
$\bar{b}$	Wing span, in
$\bar{c}$	Mean aerodynamic chord, in
n_y	Side load factor in g's
n_z	Vertical load factor in g's
p	Aircraft roll rate, rad/sec

q	Aircraft pitch rate, rad/sec
$\bar{q}$	Dynamic pressure, psi
r	Aircraft yaw rate, rad/sec
S	Wing area, in^2
ws	Wing station
α	Angle of attack, rad
β	Angle of sideslip, rad
δ_a	Deflection of aileron, rad
δ_s	Deflection of stabilator, rad
δ_r	Deflection of rudder, rad

Vector Symbols

$\{f\}$	Applied load
$\{F_g\}$	Applied load at structural grid set
$\{F_k\}$	Applied load at aerodynamic grid set
$\{F_s\}$	Static aerodynamic load
$\{F_{ss}\}$	Structural load
$\{u_g\}$	Displacement at structural grid set
$\{u_k\}$	Displacement at aerodynamic grid set
$\{u_q\}$	Rate variables set, e.g., pitch rate
$\{u_\alpha\}$	Incidence variables set, e.g., angle of attack

Matrix Symbols

$[A_{jj}]$	Aerodynamic coefficient matrix
$[D_{jk}]$	Displacement transformation matrix
$[G_{kg}]$	Interpolation matrix
$[K]$	System stiffness matrix
$[K_a]$	Aerodynamic stiffness matrix
$[K_s]$	Structural stiffness matrix
$[S_{kj}]$	Force transformation matrix

INTENTIONALLY LEFT BLANK.

1. INTRODUCTION

The technical objective of this research project is to develop flight dynamics analysis methodology for combat damaged fixed-wing aircraft to support ballistic vulnerability assessments. With combat damage, wing structural capability (stiffness/strength) can be affected. When critical structural members are weakened or destroyed, aerodynamic loadings may cause the structure to fail. In this study, removal of wing section is considered.

Removal of wing structure caused weight unbalance and the loss of the aerodynamic lifting surface. Due to the loss of a wing mass, a change of c.g. (center of gravity) occurs. The aerodynamic configurations of damaged aircraft generally involve unusual shapes, asymmetrical configurations, and possibly large angles of attack and/or sideslip for trimmed flight. Previously, standard configuration codes have been used to calculate aerodynamic stability derivatives. For example, the USAF/DATCOM and AAA (Advanced Aircraft Analysis) codes have been used for this purpose. Input for these codes comes from the geometry and the physical properties of the aircraft configuration under study. The Air Systems Branch of US Army Research Laboratory has also investigated the capability to calculate aerodynamic control and stability derivatives and trim values for damaged configurations using the MSC/NASTRAN aeroelastic code, a system of computer programs for modeling aircraft aerodynamics and structures, and for analyzing aircraft stability and loads.

The finite element structural model and aerodynamic models of the aircraft are developed individually and splined for the interpolation of deflections. Splines for both the lines and surfaces are used to generate the transformation matrix from the structural grid point deflections to the aerodynamic grid point deflections, where local streamlines are also computed. In this study, all wing skins, stabilator skins, vertical wing skins, and fuselage skins are considered as quadrilateral plate elements, and the surface spline interpolation method is used. Of particular interest is the wing-body interference option used in this report as compared to results in [1], where this option is not used.

In this study, four different subsonic Mach numbers are considered to analyze the static stabilities, aerodynamic influence coefficients, and trim values in level flight. Static longitudinal and lateral-directional stabilities are calculated and discussed for the undamaged and damaged wing configurations. The aircraft body is treated as elastic and unrestrained (free-free boundary condition). Aerodynamic influence coefficients are used to calculate the aerodynamic pressure, aerodynamic forces, and moments at subsonic speeds.

2. STATIC AEROELASTICITY

The static aeroelastic analysis involves the responses of a flexible structure to aerodynamic loading and yields the static response, stability and control derivatives, trim variables, air loads, and stresses and strains of the wing structure. All these variables are obtained for an unrestrained (free-flying) aircraft structure. The MSC/NASTRAN aeroelastic solution uses an aerodynamic influence coefficient matrix that is generated from data describing the geometry of the aerodynamic finite elements. The aerodynamic influence coefficients from the Doublet-Lattice method are used for the calculation of aerodynamic quantities in subsonic flow. This is a linearized aerodynamic potential flow theory which is presented in [2-4]. The Doublet-Lattice method with body interference is only used for the subsonic ranges. The details of the static aeroelastic analysis is explained in Appendices A-C.

3. GENERAL APPROACH TO THE PROBLEMS

The MSC/NASTRAN aeroelastic solution requires a well-designed aircraft structural model with stiffness (for static analysis) and mass balance (for dynamic analysis), and an aerodynamic model to obtain the best result. The reference geometry for the aerodynamic and structural input data is also required.

To analyze the aerodynamic effects of a damaged-wing aircraft, five different finite element wing models are examined. The first is the baseline (undamaged) and the second through fifth are for damaged wings. For the damaged cases, the right wing is examined. A full-span aerodynamic and structural model of the wing accounts for the asymmetrical configuration of the aircraft.

3.1 Description of Aircraft Model

The T-38 aircraft construction details used to model the various structural assemblies are described in [5] and [6]. See Figures 1 and 2a-c. The cantilevered wing features an aspect ratio of 3.75, no dihedral or angle of incidence relative to the fuselage, and a sweepback angle of 25° at quarter chord. The wing section has a NACA 65A004-8 (modified) airfoil. The mean aerodynamic chord is $\bar{c} = 93$ in., the chosen reference chord is $C = 80.26$ in., and the thickness/chord ratio is 4.8 %. The reference wing span is 303.0 in., and the reference area of the full-span wing is $S = 24319.1$ in^2. The horizontal stabilator has an aspect ratio of 2.85 with a mean aerodynamic chord of 43.63 in. The reference area of the horizontal stabilator is $S = 4610$ in^2. The fuselage is composed of an aluminum semi monocoque basic structure with steel, magnesium, and titanium sub-members. The fuselage length is $L_f = 582.1$ in. The weight of the wing is 1,170 lb., and the total weight of the aircraft is 11,500 lb. The moment of inertia of aircraft is $I_{xx} = 6.86 \times 10^7$(lb-in^2), $I_{yy} = 1.297 \times 10^8$ (lb-in^2), and $I_{zz} = 1.343 \times 10^8$ (lb-in^2).

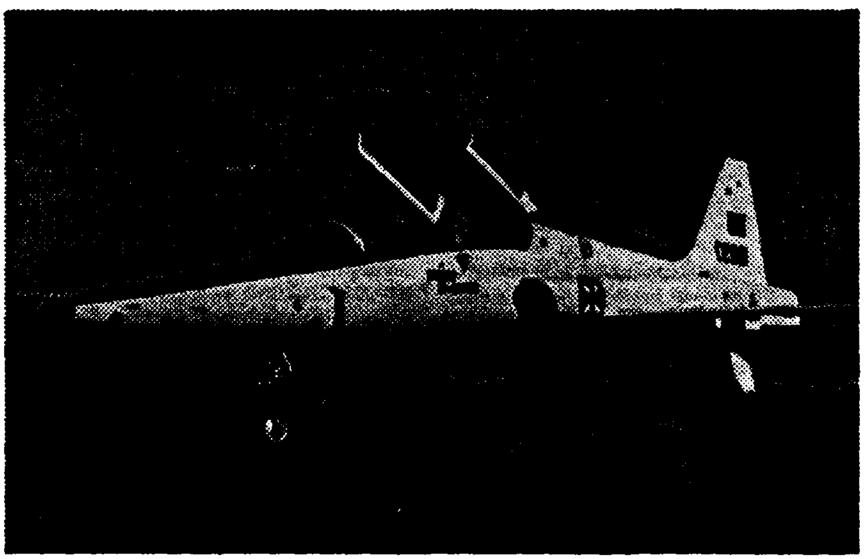

Figure 1. Real T-38 aircraft.

3.2 Structural Wing Model

Five finite element wing models are created in this report. Four damaged wing models are modified from the model baseline (undamaged aircraft). These are created by removing various regions (portions) of the aerodynamic surfaces. Damage case 1 is created by removing the internal structure and top and bottom skins of wing tip portions between w.s. 125.0 and w.s. 151.5. Damage case 2 represents more internal damage; additional spar and rib webs/chords and skins are removed between w.s. 125.0 and w.s. 111.0. Damage case 3 has additional spar and rib webs/chords and skins removed between w.s. 111.0 and w.s. 76.7. Damage case 4 has the aileron control surface alone removed. These four damage cases are shown in Figures 2d-g. The structural elements removed from the baseline finite element model to represent damage are listed in Table 1. Wing damage reduces both the wing area and the lateral distance from the aircraft centerline to the wing centerline of pressure.

To analyze the maneuvering flight of an aircraft with a damaged wing, the wing structural models (damaged and undamaged) are added to the fuselage structural model, and to the tail wing structural model group.

Table 1. Structural Element and Removed Numbers for Each Model

	Element Numbers				
MODEL / ELEMENT	Baseline	Damage 1	Damage 2	Damage 3	Damage 4
ROD	343	343	343	343	343
BEAM	276	276	256	214	276
SHEAR	136	136	125	105	136
CONROD	89	89	81	67	89
QUAD4	522	516	510	492	520
BAR	30	30	30	30	30
TRIA3	104	104	104	104	104

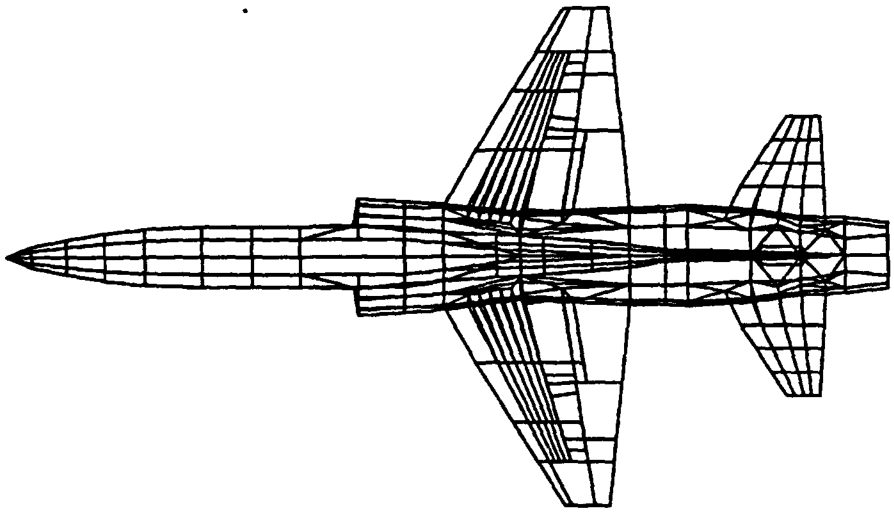

Figure 2a. Baseline finite element structural model, topview.

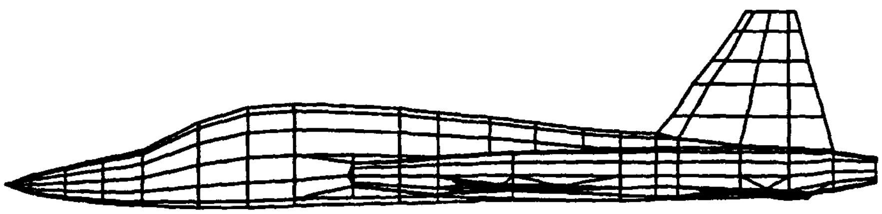

Figure 2b. Baseline finite element structural model, sideview.

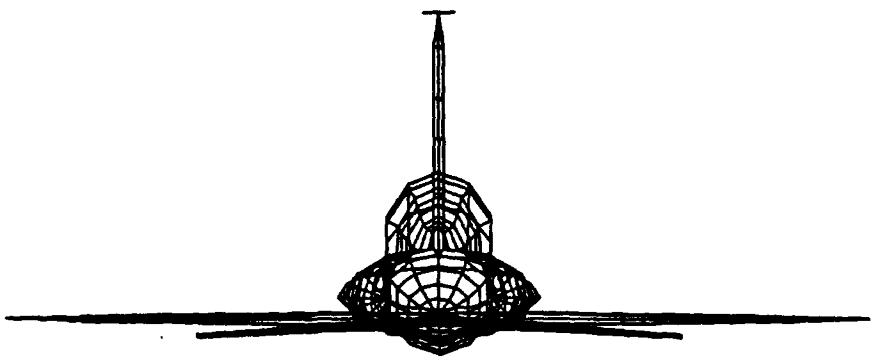

Figure 2c. Baseline finite element structural model, frontview.

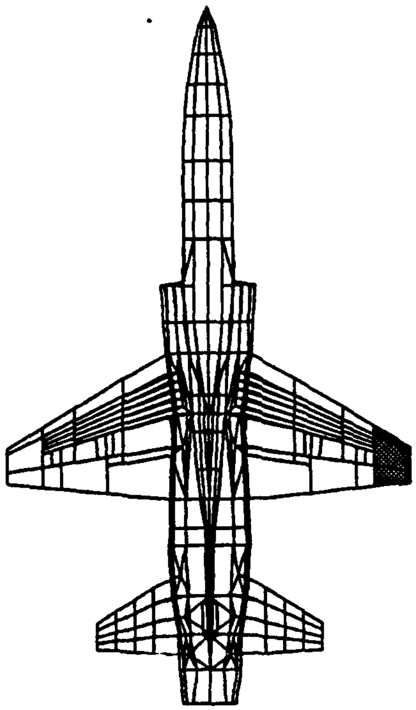

Figure 2d. Structural model damage case 1 (8.0 % right wing off).

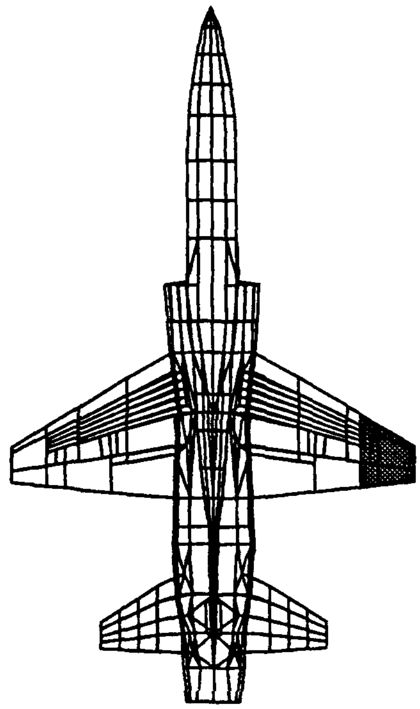

Figure 2e. Structural model damage case 2 (13.73 % right wing off).

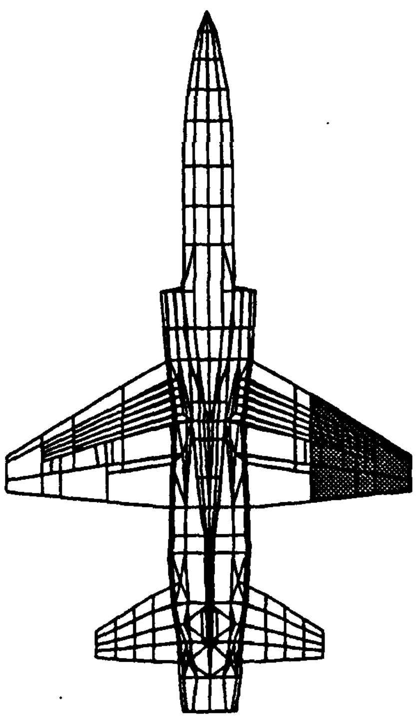

Figure 2f. Structural model damage case 3 (30.3 % right wing off).

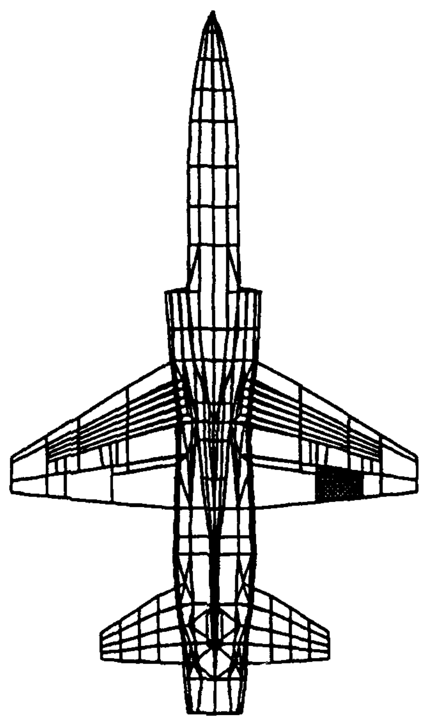

Figure 2g. Structural model damage case 4 (right aileron off).

3.3 Wing Aerodynamic Model

The wing aerodynamic model is developed using MSC/XL, initially for the aerodynamic analysis and finally (interpolated by the surface SPLINE option card in MSC/NASTRAN) for the aeroelastic analysis. In these analyses, five aerodynamic box patterns are used; the description of input data and the aerodynamic modeling technique is explained in Appendix A.

Aerodynamic models for undamaged and damaged wing cases were created in the same manner as the structural wing models. As shown in Figure 3, five cases were examined. Region 1 is defined within w.s. 0.0 (aircraft centerline) and w.s. 76.7, and within spar stations 0.0% and 100.0%. Similarly, region 2 is within w.s. 76.7 and w.s. 111.0, and spar stations 0.0% and 66.6 %. Region 3 is within w.s. 76.7 and w.s. 111.0, and spar stations 66.6% and 100.0%. Region 4 is within w.s. 111.0 and w.s. 125.0, and spar stations 0.0% and 100.0 %. Region 5 is within w.s. 125.0 and w.s. 151.5, and spar stations 0.0 % and 100.0 %.

Region 5 is removed for damage case 1. Regions 4 and 5 are removed for damage case 2. The wing tip station is changed from 151.5 to 125.0 for case 1 and to 111.0 for case 2. Regions 2, 3, 4, and 5 are removed for damage case 3. Region 3 is removed for damage case 4. For the damage case 4, the wing tip station is changed from 151.5 to 76.7. Aerodynamic boxes are located on the remaining wing and tail surfaces. The corresponding aerodynamic models are shown in Figures 4a-g.

3.4 Wing-Body Interference

Since this study is concerned with lifting surfaces, the fuselage is represented as a beam and the aerodynamic effects of the fuselage are neglected (i.e., it is assumed that there are no aerodynamic forces acting on the fuselage).

The fuselage body is further idealized as slender with interference elements. The primary purpose of the slender body elements is to account for the forces arising from the motion of the fuselage, whereas the interference elements are used to account for interference among all bodies and panels in the same group. This is done by providing a surface through which the boundary

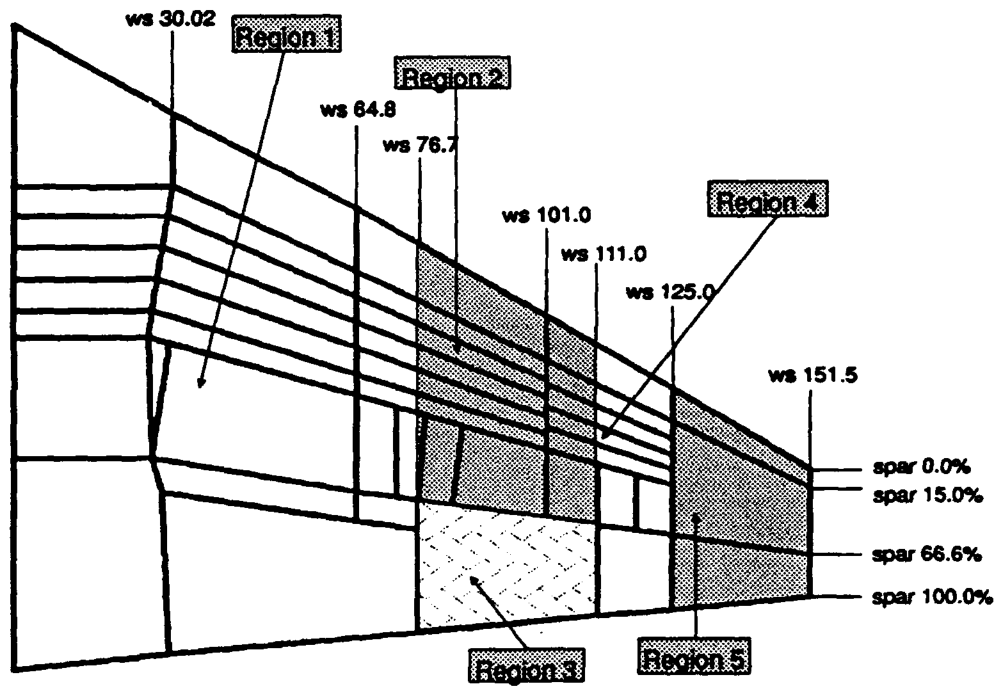

Figure 3. Designation of removed region of wing structure.

condition of no flow is imposed. Bodies are further classified as to the type of motion allowed. In the aerodynamic coordinate system, y and z are perpendicular to the flow. In general, bodies may move in both the y-(lateral) and z-(vertical) directions. Frequently, a body (i.e., a fuselage) lies on a plane of symmetry and only z-(or y-) motion is allowed. Thus, this model contains zy-bodies. One or two planes of symmetry or antisymmetry may be specified. Figure 5 shows an idealization for determining the effect of the wing on itself and other parts of the aircraft. More details of wing-body (fuselage) interference used in this study are described in [7].

3.5 Control Surfaces

The aircraft control surface deflections are defined by the conventional symbols δ_s, δ_a, and δ_r for pitch, roll, and yaw control, respectively. The pitch control deflection δ_s is defined as a symmetric

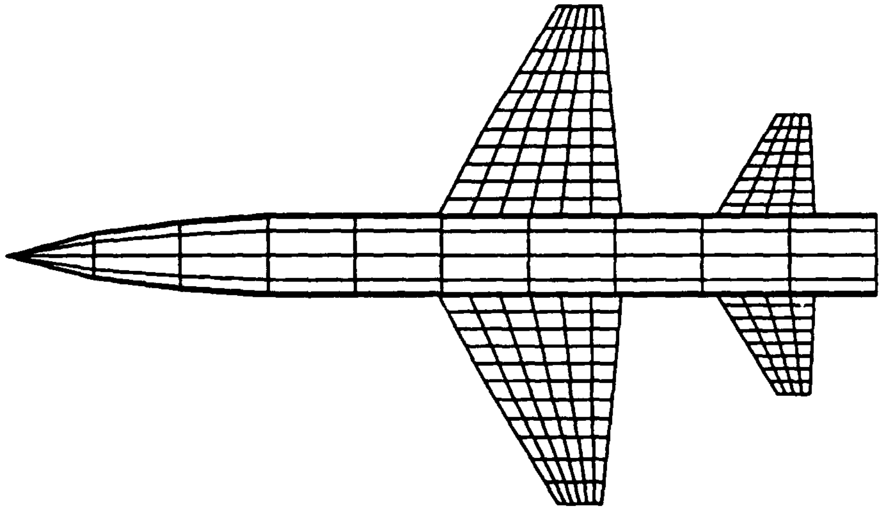

Figure 4a. Baseline aerodynamic model, topview.

Figure 4b. Baseline aerodynamic model, sideview.

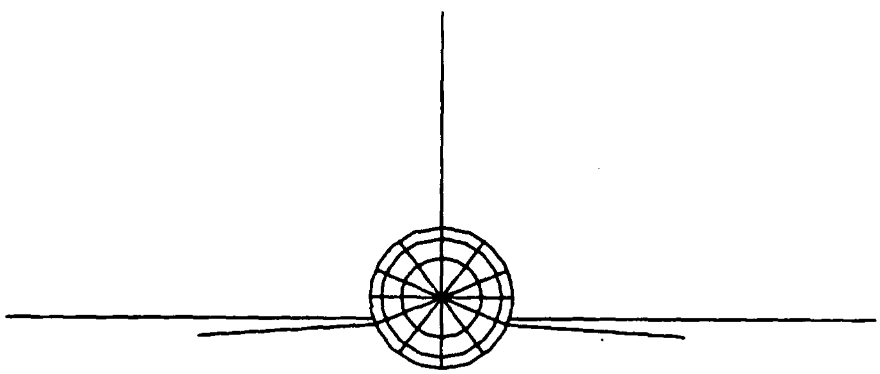

Figure 4c. Baseline aerodynamic model, frontview.

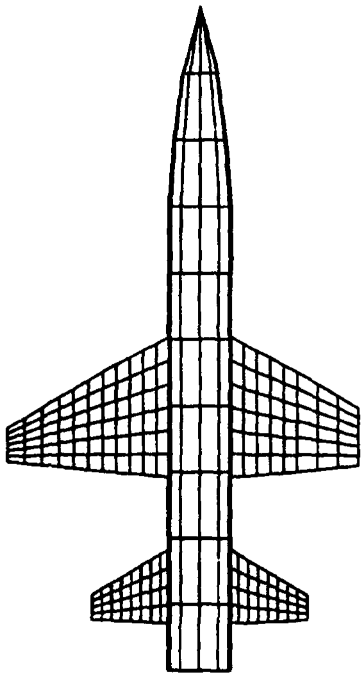

Figure 4d. Aerodynamic model damage case 1 (8.0 % right wing off).

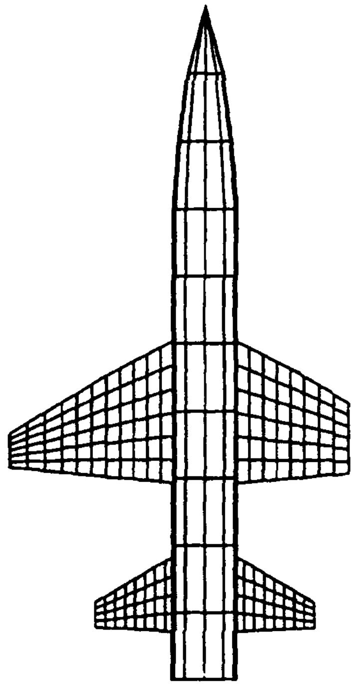

Figure 4e. Ae dynamic model damage case 2 (13.73 % right wing off).

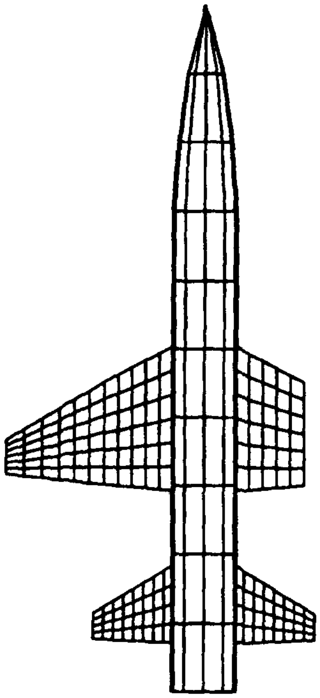

Figure 4f. Aerodynamic model damage case 3 (30.3 % right wing off).

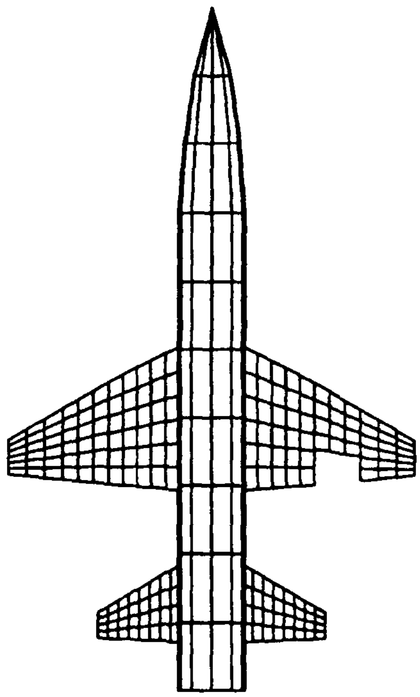

Figure 4g. Aerodynamic model damage case 4 (right aileron off).

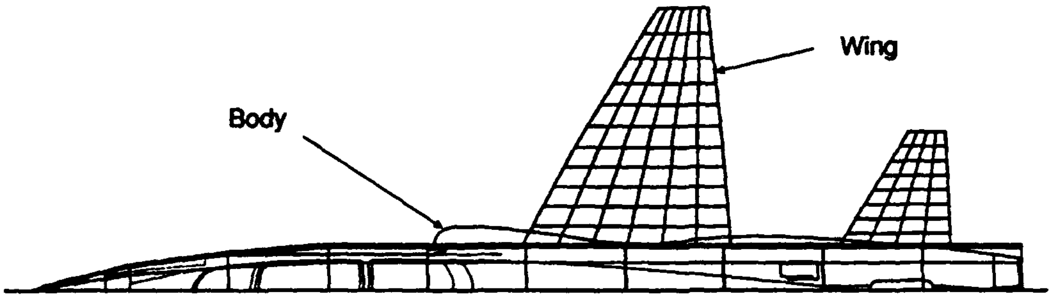

Figure 5. Idealized interference wing and body.

equal deflection of the left and right horizontal tail surface (stabilator), while the roll control deflection δ_a is defined as an antisymmetric deflection of the ailerons. Yaw control deflection δ_r is defined by rotation of rudder.

Positive aileron deflection is defined as left aileron trailing edge down, right aileron trailing edge up, and produces a positive rolling moment. Since the left and right stabilators rotate together(one-piece all moving tail) the positive rotation is defined as the leading edge down for both sides and produces a nose-up control moment. A trailing edge left rudder rotation gives a positive side force from the rudder. The control deflection δ_a(aileron), δ_s(stabilator), and δ_r(rudder) are defined as positive when they introduce positive force contributions along the X, Y, and Z axes, respectively, at small angles of attack and sideslip conditions. Sign convention for control surface deflections are shown in Figures 6a-c.

4. AEROELASTIC ANALYSIS

The aerodynamic analysis, like the structural analysis, is based on a finite element approach. The finite aerodynamic elements are strips or boxes on which there are aerodynamic forces. There

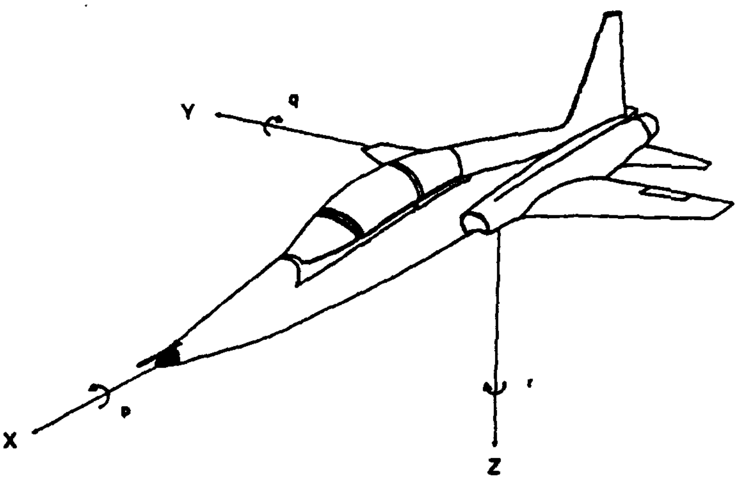

Figure 6a. Aircraft axis system.

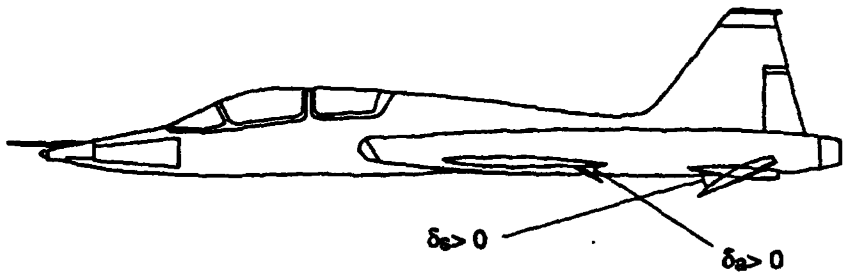

Figure 6b. Sign symbols for stabilator and aileron deflections.

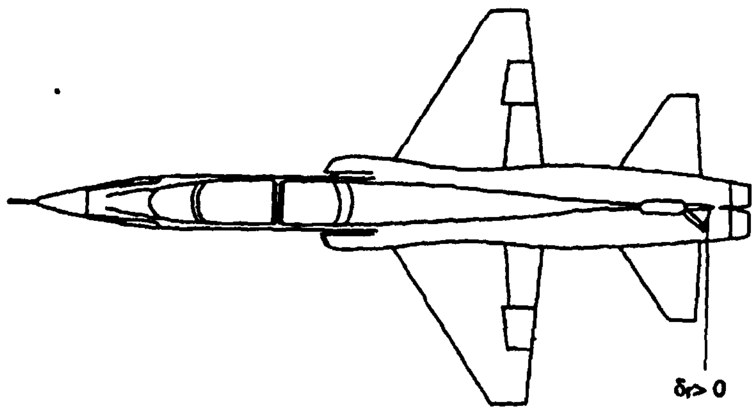

Figure 6c. Sign symbol for rudder deflection.

are two major points to be considered. The aerodynamic elements, even for rather complex vehicles, tend to be regular arrays. Thus, MSC/NASTRAN aeroelastic solution generates the arrays of aerodynamic elements. In particular, the aerodynamic elements for the lattice methods are arrays of trapezoidal boxes whose sides are parallel to the airflow. These can be described simply by defining properties of the array (panel). Because the grid points defining the structural elements usually will not coincide with the grid points defining the aerodynamic elements, provision has been made to generate equations for interpolating from the former to the latter. This interpolation is a key feature since it allows the choice of structural and aerodynamic elements to be based on structural and aerodynamic considerations independently.

Unsteady aerodynamic forces are generated when the flow is disturbed by the moving (elastic) structure, or when the flow itself is unsteady, as in the case of atmospheric turbulence. In the former case, theory leads to a matrix that relates the forces acting on the structure to the deflections of the structure. State-of-the-art methods which involve interactions among aerodynamic elements are available only for steady-state sinusoidal motion.

4.1 Interconnection of the Structure with Aerodynamics

There are two sets of displacements for the analysis of static aeroelasticity in MSC/NASTRAN. One set is the dependent displacements set, u_k, which is determined at a set of points whose location is determined by the aerodynamic theory. The other set is the independent structural displacements set, u_g, which consists of structural grid point displacements in the global coordinate system. The dependent displacements, u_k, are interpolated from the structural displacement u_g by the following relation.

$$\{u_k\} = [G_{kg}]\{u_g\} \tag{1}$$

In order to obtain the interpolation matrix $[G_{kg}]$, three types of splines are available in MSC/NASTRAN. These are out-of-plane surfaces spline, out-of-plane linear spline, and in-plane linear spline. Out-of-plane motion consists of displacements normal to the plane, and rotations about axes parallel to the plane. In this study, out-of-plane displacements (normal displacement) over the wing surface, stabilator surface, and vertical fin surface are interpolated by using the above equation (1). Therefore, the out-of-plane surface spline is used for this analysis. The detailed explanation of a surface spline method is given in [8].

4.2 Response Solution

The structural equation is

$$[K_s]\{u_g\} = \{F\} \tag{2}$$

where $[K_s]$ is the structural stiffness matrix, $\{u_g\}$ is the displacement vector, and $\{F\}$ is the applied load vector. The force and moments are represented by

$$\{F\} = \{F_k\} + \{F_g\} \tag{3}$$

where $\{F_k\}$ is the applied load vector that contributes to rigid body motions and control surfaces, and $\{F_g\}$ is the additional load vector due to the change from the original deformation (structural deformation). The aerodynamic force vectors applied at rigid body motions and control surfaces and at structural grid points are given as

$$\{F_k\} = \bar{q}[S_{kj}][A_{jj}]^{-1}[D_{jk}]\{u_k\} \tag{4}$$

$$\{F_g\} = \bar{q}[G_{kg}]^T[S_{kj}][A_{jj}]^{-1}[D_{jk}][G_{kg}]\{u_g\} \tag{5}$$

where $\bar{q}$ is dynamic pressure, $[S_{kj}]$ is a force transformation matrix, and $[D_{kj}]$ is a displacement transformation matrix. The force vector $\{F_k\}$ is composed of two loads,

$$\{F_k\} = \{F_{ss}\} + \{F_s\} \tag{6}$$

where $\{F_{ss}\}$ is a structural load vector, and $\{F_s\}$ is a static aerodynamic force vector; primarily, the force determined by the planform and airfoil configuration of the wing and the angle of attack.

The flexible wing geometry can be expressed in terms of translational and rotational deflection vectors,

$$\{u\} = \{u_k\} + \{u_g\} \tag{7}$$

where $\{u_k\}$ is the undeformed vector at the aerodynamic gird points and $\{u_g\}$ is the elastic deformation vector at the structural grid points.

From equation (2) through (5), we obtain

$$[K_s]\{u_g\} = \{F_k\} + \bar{q}[G_{kg}]^T[S_{kj}][A_{jj}]^{-1}[D_{kj}][G_{kg}]\{u_g\} \tag{8}$$

Rearranging equation (8), we get

$$[K]\{u_g\} = \{F_k\} \tag{9}$$

where the system stiffness matrix [K] is defined as

$$[K] = [K_s] - [K_a] \tag{10}$$

and the aerodynamic stiffness matrix, $[K_a]$ is defined as

$$[K_a] = \bar{q}[G_{kg}]^T[S_{kj}][A_{jj}]^{-1}[D_{kj}][G_{kg}] \tag{11}$$

The aeroelastic response solutions are obtained from equation (9).

5. AERODYNAMIC STABILITY DERIVATIVES

Stability derivatives are aerodynamic coefficients nondimensionalized by reference geometry appropriate to the specified derivative. The size of the nondimensional derivatives is normalized with respect to aircraft and flight conditions. The MSC/NASTRAN aeroelastic solution provides a complete set of aerodynamic estimates, usually as a function of angle of attack for the various flight conditions. For various angles of attack, the downwash equation $\{W^a_j\}$, W2GJ is listed on the MSC/NASTRAN DMI card option (See [9] for more details). In the longitudinal case, the angle of attack, α, and stabilator deflection, δ_s, are the two incidence variables,

$$\{u_\alpha\} = \begin{Bmatrix} \alpha \\ \delta_s \end{Bmatrix} \tag{12}$$

$$[m_r][M^s_{rr}]^{-1}[K_{r\alpha}] = -\bar{q}S\begin{bmatrix} C_{z_\alpha} & C_{z_\delta} \\ C_{m_\alpha}\bar{c} & C_{m_\delta}\bar{c} \end{bmatrix} \tag{13}$$

where S and $\bar{c}$ are the reference area and chord, respectively. The factor $[m_r][M^s_{rr}]^{-1}$ introduces the inertial relief effects into the unrestrained derivatives. For the case of longitudinal pitching with pitch rate q,

$$\{u_q\} = \left(\frac{q\bar{c}}{2V}\right) \tag{14}$$

and

$$[m_r][M^r_{rr}]^{-1}[K^s_{rq}] = -\bar{q}S\begin{Bmatrix} C_{z_q} \\ C_{m_q}\bar{c} \end{Bmatrix} \tag{15}$$

Similar relationships are available for the lateral-directional stability derivatives. The rigid stability derivatives are appropriately found by the user's selection of a small value of $\bar{q}$ and do not need any special consideration.

5.1 Longitudinal Stability Derivatives

A characteristic of fixed-wing aircraft longitudinal stability is the tendency to maintain the trim angle of attack. Longitudinal stability derivatives are determined by the aircraft mass, inertia aerodynamic, and geometric layout parameters. The most important derivatives for conventional aircraft are: C_{l_α}, C_{m_q}, C_{m_α}, and $C_{m_{\dot{\alpha}}}$. A summary of these longitudinal terms is given in Table 2.

Table 2. Summary of Longitudinal Terms

Terms	Symbol	Description	Affected By
Longitudinal Static Stability	C_{m_α}	Tendency of aircraft to return to trim angle of attack	Size, location of stabilator, wing pitching moment, and fuselage component and relative positions of c.g. and center of lift once configuration is fixed

Pitch Damping Coefficient	C_{m_q}	A measure of the moment resisting pitching motion	Size and location of stabilator and air density
Angle of Attack Damping Coefficient	$C_{m_{\dot{\alpha}}}$	A measure of the moment created due to delay of downwash effect on tail after wing angle of attack has been changed	Size and location of stabilator in relation to wing
Lift Curve Slope	C_{z_α}	Lift force due to change in angle of attack (wing or tail)	Area, airfoil shape, aspect ratio and sweepback angle of wing or tail

5.2 Lateral-Directional Stability Derivatives

Lateral-directional stability is generally coupled for fixed-wing aircraft. For example, while longitudinal motion is restricted to a single axis (pitch), the lateral-directional motion involves two axes (roll and yaw). Also, longitudinal stability derivatives all pertain to the pitch axis, whereas certain lateral and directional derivatives are coupled between the roll and yaw axis. Single derivative variation can drastically impact the lateral-directional stability. The most important lateral-directional stability derivatives for conventional aircraft are C_{l_β}, C_{n_β}, C_{l_p}, C_{n_p}, C_{l_r}, C_{n_r}, and C_{y_β}. A summary of these lateral-directional terms is given in Table 3.

Table 3. Summary of Lateral-Directional Terms

Term	Symbol	Description	Affected By
Directional Static Stability Coefficient	C_{n_β}	Tendency of aircraft to align (weather clock) into relative wind	Primarily vertical tail area and distance aft of c.g. and side area distribution force
Yaw Damping Coefficient	C_{n_r}	Yawing moment coefficient due to yaw rate. Created by β changes due to the rotational velocity. Acts in a direction to oppose yaw rate (similar in concept to pitch damping coefficient and roll damping coefficient)	Size and placement of vertical tail and air density

Yaw due to Lateral Control Coefficient	$C_{n_{\delta_a}}$	Yawing moment coefficient due to unbalanced drag of wings with aileron deflection. Adverse yaw away from desired turn. Proverse yaw into desired turn	Type of lateral control (aileron, etc) and control size and distance from c.g.. May affected by angle of attack as airflow over vertical tail is blanked. Effect can be minimized with aileron/rudder interconnect
Yaw due to Roll Rate Coefficient	C_{n_p}	Yawing moment coefficient due to rotation of lift vectors of each wing during roll	Wingspan and lift curve slope (C_L vs. α)
Rudder Effectiveness Coefficient	$C_{n_{\delta_r}}$	Yawing moment coefficient due to rudder deflection	Rudder surface area and distance of rudder from c.g.
Dihedral Effect	C_{l_β}	Rolling moment coefficient due to sideslip. Positive dihedral - roll away from sideslip. Negative dihedral - roll toward sideslip angle	Geometric dihedral of wings, location of wings on fuselage, and effect often vary with angle of attack
[1]Roll Damping Coefficient	C_{l_p}	Rolling moment coefficient due to roll rate. Created by α changes due to the rotational velocity "p". Acts in a direction to oppose roll rate (similar in concept to pitch damping coefficient and yaw damping coefficient)	Lift curve slope (C_L vs. α), wingspan and area, and air density
Roll due to Yaw Rate Coefficient	C_{l_r}	Rolling moment coefficient created by one wing moving through air faster than other when aircraft yawed	Lift curve slope (C_L vs. α), and wingspan
[2]Roll due to Rudder Deflection Coefficient	$C_{l_{\delta_r}}$	Rolling moment coefficient due to force on rudder surface not acting through roll axis	Rudder surface area and vertical location of rudder
Aileron Effectiveness Coefficient	$C_{l_{\delta_a}}$	Rolling moment coefficient due to aileron deflection	Aileron surface area and distance from ailerons to roll axis
Side Force Coefficient	C_n	Side-force derivative coefficient due to sideslip	Fuselage shape and aircraft geometric layout

NOTE: [1]Determines roll mode time constant (how quickly roll rate reaches steady state)

[2]Usually a minor coupling factor on most aircraft

5.3 Definition of Force and Moment Coefficients

The principle force and moment coefficients are the: lift coefficient, C_L; rolling moment coefficient, C_l; pitching moment coefficient, C_m; yawing moment coefficient, C_n; and the normal and axial force coefficients, C_z and C_x. The longitudinal derivatives and the lateral derivatives are provided as the output as shown in Tables 4-7. Also, the MSC/NASTRAN aeroelastic solution has the capability of computing the aerodynamic stability derivatives for control surface deflection.

Aerodynamic coefficients and derivatives are used to calculate the aerodynamic forces and moments acting on the aircraft. Due to the strong dependence of the C_{z_α} and C_{m_α} derivatives on the angle of attack, they are represented as angle of attack dependent coefficients so that:

$$C_{m_1} = C_{m_\alpha}\alpha \tag{16}$$

$$C_{L_1} = C_{z_\alpha}\alpha \tag{17}$$

and the lift coefficient is

$$C_L = C_{L_1} + C_{z_{\delta_s}}\delta_s + C_{z_q}q \tag{18}$$

5.3.1 Baseline Aircraft Configuration

Aerodynamic force and moment expansions of the baseline aircraft configuration result in the classical description of the symmetrical aircraft where the longitudinal and lateral directional forces and moments are developed independently. The baseline aircraft is described by the following force and moment coefficients.

$$C_y = C_{y_\beta}\beta + C_{y_{\delta_a}}\delta_a + C_{y_{\delta_r}}\delta_r + C_{y_p}p + C_{y_r}r \tag{19a}$$

$$C_z = C_{z_0} + C_{z_\alpha}\alpha + C_{z_{\delta_s}}\delta_s + C_{z_q}q \tag{19b}$$

$$C_l = C_{l_\beta}\beta + C_{l_{\delta_a}}\delta_a + C_{l_{\delta_r}}\delta_r + C_{l_p}p + C_{l_r}r \tag{19c}$$

$$C_n = C_{n_\beta}\beta + C_{n_{\delta_a}}\delta_a + C_{n_{\delta_r}}\delta_r + C_{n_p}p + C_{n_r}r \tag{19d}$$

5.3.2 Asymmetric Wing Damage Configuration

Aerodynamic force and moment expansions for the asymmetric wing damage configuration represent a significant departure from the baseline aircraft. This configuration is characterized by considerable pitch/yaw coupling which is reflected in the aerodynamic model which is presented below.

$$C_y = C_{y_\beta}\beta + C_{y_{\delta_a}}\delta_a + C_{y_{\delta_r}}\delta_r + C_{y_p}p + C_{y_r}r \tag{20a}$$

$$C_z = C_{z_0} + C_{z_\alpha}\alpha + C_{z_\beta}\beta + C_{z_{\delta_a}}\delta_a + C_{z_{\delta_s}}\delta_s + C_{z_q}q \tag{20b}$$

$$C_l = C_{l_\alpha}\alpha + C_{l_\beta}\beta + C_{l_{\delta_a}}\delta_a + C_{l_{\delta_r}}\delta_r + C_{l_p}p + C_{l_q}q + C_{l_r}r \tag{20c}$$

$$C_n = C_{n_\beta}\beta + C_{n_{\delta_a}}\delta_a + C_{n_{\delta_r}}\delta_r + C_{n_p}p + C_{n_r}r \tag{20d}$$

As shown in the above equations, to calculate the rolling moment coefficient of asymmetric wing damage aircraft, two more terms, $C_{l_\alpha}\alpha$ and $C_{l_q}q$, are added to Eq. (19c) and are shown in Eq. (20c). Two terms, C_{l_α} and C_{l_q}, are near to zero for undamage wing (baseline) as shown in Tables 4-7. So we can neglect these two terms for Eq. (19c).

6. DISCUSSION OF RESULTS

Results are obtained for five aircraft models, one baseline (undamaged) and four with asymmetric wing damages. Four subsonic Mach numbers at a sea level flight condition are considered, resulting in the dynamic pressures values listed in Table 8.

The level flight condition was modeled after that of [9]. The trim solution is obtained only for subsonic flight in quasi-steady equilibrium. In this study, the pitch rate, rudder deflections, pitch accelerations, roll accelerations, yaw accelerations, lateral accelerations, and vertical accelerations, are all set to zero. Also, to compare the damage case 4 (aileron removed) with the baseline case and the other three damage cases, aileron deflections are also set to zero. With these input trim conditions, the angle of attack, sideslip angle, stabilator rotation, roll rate, and yaw rate are determined.

Table 9 shows static aeroelastic effects between the five cases. Results are obtained for a 10° angle of attack and a Mach number of 0.7. The maximum deflection is 4.5168 in. for the baseline wing and 2.3947 in. for wing damage case 3. The rolling moment coefficient is smallest for the baseline and increases with wing damage. This change is due to the different aerodynamic load distributions on the wing surfaces. The lift coefficient calculation is based on equation (18). Lift coefficient varies linearly with wing damage due to the loss of lifting surface.

Table 10 shows trim values for the five cases at Mach 0.7. Here the roll rate(p) and yaw rate(r) increase with wing damage. It is shown that wing damage results in a higher roll and yaw rate than the baseline wing for trimmed flight.

The effects of wing damage on the aerodynamic coefficients and derivatives are shown in Tables 4-7 at Mach numbers 0.4, 0.5, 0.6, and 0.7 at an angle of zero lift. Among the variables shown in this table, C_{l_α}, C_{l_q}, and C_{m_p} are the most significantly affected. This is largely due to longitudinal/lateral coupling effects. These terms are near zero for the baseline aircraft.

Table 11 shows the effects of normal longitudinal coupling as compared with lateral-directional motions. Two typical derivatives, C_{m_α} and C_{m_q}, are listed in this table. The increments of weight loss due to damaged wings and their locations produce asymmetric inertial terms and changes the normal axes system (the center of gravity). With the changes in aircraft weight and inertia due to removal of wing structure, changes in aerodynamic coefficient derivatives are expected.

Figure 7 shows the aileron effectiveness. The rolling moment due to aileron deflection is significantly affected by aileron area removal (or distance from aileron to roll axis). For damage cases 3 and 4, the entire right aileron is removed.

Figure 8 shows that wing damage causes a reduction in lift slope with very little change in the angle of zero lift. Although the wing is considered as elastic, the lift coefficient is linear for this angle of attack range.

Figure 9 shows the changes in the lift curve slope with respect to the angle of attack, α, for the baseline and the four damaged wing configurations. It is shown that this term increases with Mach number.

Comparison of wing damage data in Figures 10a-b, 11a-b, and 12a-b shows large systematic changes in the rolling moment (C_l) which are dependent mainly on angle of attack α. At α= 5.0°, Figure 10b shows increased rolling moments as outboard portions of the wing are removed. Damage case 3 (30.3 % right wing off) has the largest rolling moment among the four cases. This trend was not observed for small α as shown in Figure 10a (α=0.4°). While yaw[illegible]n moment and side force are not affected by angle of attack for the damage wing configurations.

The yawing moment coefficient C_n, shown in Figures 11a-b, is of particular interest: the side force coefficient C_y, shown in Figures 12a-b, changes very little, and the rolling moment coefficients behave as would have been expected; that is, increasing lift with the lateral center of pressure moved to the left of the origin would be expected to increase the rolling moment. The quite regular reduction in the lift coefficient slope with respect to the angle of attack for the baseline aircraft and the four wing damage configurations are summarized in Figure 9.

Figures 13a-b show that with sideslip, there is very little influence on pitching moment coefficient. Figure 13b also shows that (at Mach 0.7 and α=5.0°) wing damage significantly influenced the pitching moment.

Wing damage reduces both the wing area and the lateral distance from the aircraft centerline to the wing center of pressure. The rolling moment is calculated as the difference in the products of the lift and distance to the spanwise center of pressure for the damaged and undamaged wings. The calculated rolling moment coefficient for the baseline and the four damaged-wing aircraft is plotted in Figure 14 at Mach = 0.4, 0.5, 0.6, and 0.7, and at an angle of attack of 10.0°.

The most important effect of wing damage is shown in Figures 15-17, where the rolling moment coefficient is seen to be strongly affected by angle of attack. The rolling moment coefficients (C_l), pitching moment coefficients (C_m), and yawing moment coefficients (C_n) are plotted vs. sideslip angle for three different angles of attack at M=0.7 for the damage case 3 (30.3 % right wing off) and the baseline aircraft. At angles of attack of 0.4°, 5.0°, and 10.0°, the baseline aircraft rolling moment is not changed. The three baseline curves are all at the same location. However, the rolling moment with damage increases with angle of attack. It is shown that the slope of the rolling moment coefficient vs. sideslip (C_{l_β}) is not greatly affected by wing damage or angle of attack even though the magnitude of the induced rolling moment increases significantly. For the baseline aircraft, the C_l vs. β variation is shown to be insensitive to angle of attack from zero to 10° with a C_{l_β} value of approximately -0.096112.

Figure 16 shows that the pitching moment (C_m) is reduced with angle of attack and wing damage due to reduction in total lift and shift of the center pressure. Also, the pitching moment is influenced very little by the amount of sideslip. Figure 17 shows that the yawing moment coefficient (C_n) is strongly affected by sideslip, but not by wing damage.

Figures 18a and 18b show the damping-in-roll as an elastic wing and rigid wing for the baseline and damage cases at Mach numbers of 0.4, 0.5, 0.6, and 0.7. Flexibility effects increase with Mach number for all cases.

Table 4. Aerodynamic Coefficient Derivatives at Mach 0.4

Mach = 0.4					
Model	Baseline	Damage 1	Damage 2	Damage 3	Damage 4
C_{z_α}	4.21504E+00	3.79706E+00	3.52388E+00	2.91184E+00	4.04093E+00
C_{z_q}	-9.57821E+00	-8.94627E+00	-8.51241E+00	-7.57379E+00	-9.06388E+00
$C_{z_{\delta_a}}$	-7.84992E-06	4.17877E-02	-7.39723E-02	-2.58857E-01	-2.73841E-01
$C_{z_{\delta_s}}$	5.71944E-01	5.69672E-01	5.67432E-01	5.62092E-01	5.70935E-01
C_{m_α}	-1.44600E+00	-1.22174E+00	-1.08762E+00	-1.00846E+00	-1.35119E+00
C_{m_p}	-7.10711E-04	1.41237E-01	1.98113E-01	2.28794E-01	3.58894E-02
C_{m_q}	-1.01680E+01	-9.81845E+00	-9.58419E+00	-9.35982E+00	-9.89418E+00
$C_{m_{\delta_a}}$	2.38867E-04	2.72647E-02	-4.23605E-02	-1.39133E-01	-1.444948E-01
$C_{m_{\delta_s}}$	1.37514E+00	1.37474E+00	1.37356E+00	1.37260E+00	1.37545E+00
C_{l_α}	1.67761E-04	1.26804E-01	1.89476E-01	2.82202E-01	3.57967E-02
C_{l_β}	-7.81310E-02	-7.74624E-02	-7.85118E-02	-7.85176E-02	-7.85873E-02
C_{l_p}	-3.61364E-01	-2.83867E-01	-2.52809E-01	-2.21798E-01	-3.48072E-01
C_{l_q}	7.40125E-04	1.94531E-01	2.90100E-01	4.36061E-01	1.04029E-01
C_{l_r}	9.74985E-02	9.66311E-02	9.71206E-02	9.73714E-02	9.80339E-02
$C_{l_{\delta_a}}$	1.10443E-01	1.18387E-01	8.84361E-02	5.67570E-02	5.59648E-02
$C_{l_{\delta_s}}$	-1.56579E-04	-1.12863E-03	-1.59978E-03	-2.34888E-03	-5.31615E-04
$C_{l_{\delta_r}}$	4.56876E-02	4.51982E-02	4.51368E-02	4.52327E-02	4.58502E-02
C_{y_β}	-4.10707E-01	-4.10931E-01	-4.10817E-01	-4.11054E-01	-4.10737E-01
C_{y_p}	-1.08371E-01	-1.15468E-01	-1.20547E-01	-1.29159E-01	-1.11145E-01
$C_{y_{\delta_r}}$	2.07602E-01	2.07735E-01	2.07793E-01	2.07911E-01	2.07636E-01
C_{n_α}	2.33317E-05	5.43758E-03	9.58457E-03	2.04680E-02	3.14829E-03
C_{n_β}	2.00311E-01	2.00420E-01	2.00366E-01	2.00483E-01	2.00323E-01
C_{n_p}	5.44556E-02	5.79462E-02	6.03200E-02	6.42365E-02	5.57621E-02
C_{n_q}	-2.68094E-04	7.97308E-03	1.42244E-02	3.10524E-02	9.07929E-03
C_{n_r}	-2.59213E-01	-2.59351E-01	-2.59358E-01	-2.59479E-01	-2.59231E-01
$C_{n_{\delta_a}}$	9.95017E-03	1.06599E-02	8.17248E-03	4.77960E-03	5.01351E-03
$C_{n_{\delta_s}}$	6.86758E-05	1.52971E-05	-2.24133E-05	-1.33222E-04	2.33446E-05
$C_{n_{\delta_r}}$	-1.22296E-01	-1.22362E-01	-1.22390E-01	-1.22447E-01	-1.22311E-01

Table 5. Aerodynamic Coefficient Derivatives at Mach 0.5

Mach = 0.5					
Model	Baseline	Damage 1	Damage 2	Damage 3	Damage 4
C_{z_α}	4.57659E+00	4.10584E+00	3.81836E+00	3.17836E+00	4.37825E+00
C_{z_q}	-1.16997E+01	-1.09620E+01	-1.05282E+01	-9.49412E+00	-1.11010E+01
$C_{z_{\delta_a}}$	-1.45461E-04	4.76725E-02	-8.13686E-02	-2.79884E-01	-2.88440E-01
$C_{z_{\delta_s}}$	1.06051E+00	1.04891E+00	1.04221E+00	1.02540+00	1.05214E+00
C_{m_α}	-1.77552E+00	-1.50672E+00	-1.35713E+00	-1.27100E+00	-1.65597E+00
C_{m_p}	-2.85686E-04	1.66015E-01	2.34028E-01	2.63505E-01	4.18294E-02
C_{m_q}	-1.31054E+01	-1.26693E+01	-1.24240E+01	-1.21474E+01	1.27511E+01
$C_{m_{\delta_a}}$	4.83714E-04	3.36043E-02	-4.91299E-02	-1.62964E-01	-1.64722E-01
$C_{m_{\delta_s}}$	2.10135E+00	2.09495E+00	2.09133E+00	2.08780E+00	2.09689E00
C_{l_α}	-1.96970E-04	1.35930E-01	2.05927E-01	3.00117E-01	3.91342E-02
C_{l_β}	-7.73243E-02	-7.67339E-02	-7.59866E-02	-7.64892E-02	-7.79386E-02
C_{l_p}	-3.81447E-01	-2.96990E-01	-2.64953E-01	-2.35036E-01	-3.67553E-01
C_{l_q}	-5.36550E-04	2.07862E-01	3.19944E-01	4.75023E-01	1.14177E-01
C_{l_r}	9.69865E-02	9.57009E-02	9.52461E-02	9.58319E-02	9.77153E-02
$C_{l_{\delta_a}}$	1.12176E-01	1.19102E-01	9.15306E-02	5.90544E-02	5.70152E-02
$C_{l_{\delta_s}}$	1.05286E-04	-2.98373E-03	-4.62703E-03	-6.92125E-03	-1.35028E-03
$C_{l_{\delta_r}}$	4.75004E-02	4.66213E-02	4.64843E-02	4.66492E-02	4.77401E-02
C_{y_β}	-4.15889E-01	-4.16073E-01	-4.16317E-01	-4.16513E-01	-4.15912E-01
C_{y_p}	-1.06301E-01	-1.54147E-01	-1.19302E-01	-1.27519E-01	-1.09260E-01
$C_{y_{\delta_r}}$	2.11482E-01	2.11673E-01	2.11759E-01	2.111908E-01	2.11521E-01
C_{n_α}	2.05693E-06	5.61868E-03	1.04268E-02	2.07636E-02	3.39101E-03
C_{n_β}	2.02486E-01	2.02581E-01	2.02670E-01	2.02802E-01	2.02496E-01
C_{n_p}	5.36605E-02	5.75998E-02	5.99385E-02	6.36624E-02	5.50501E-02
C_{n_q}	-4.46927E-04	7.86724E-03	1.57873E-02	3.30885E-02	9.84587E-03
C_{n_r}	-2.62616E-01	-2.62779E-01	-2.62887E-01	-2.63021E-01	-2.62633E-01
$C_{n_{\delta_a}}$	9.94729E-03	1.03764E-02	8.64933E-03	5.04588E-03	5.01822E-03
$C_{n_{\delta_s}}$	1.02969E-04	-4.80167E-05	-1.80294E-04	-4.92736E-04	-5.13809E-05
$C_{n_{\delta_r}}$	-1.25256E-01	-1.25351E-01	-1.25394E-01	-1.25469E-01	-1.25273E-01

Table 6. Aerodynamic Coefficient Derivatives at Mach 0.6

Mach = 0.6					
Model	Baseline	Damage 1	Damage 2	Damage 3	Damage 4
C_{z_α}	4.69352E+00	4.19492E+00	3.89357E+00	3.32482E+00	4.50114E+00
C_{z_q}	-1.13998E+01	-1.06459E+01	-1.02122E+01	-9.32184E+01	-1.08420E+01
$C_{z_{\delta_a}}$	3.58901E-04	4.79920E-02	-8.09298E-02	-2.59486E-01	-2.64279E-01
$C_{z_{\delta_s}}$	8.53428E-04	8.44764E-01	8.40099E-01	8.30662E-01	8.48295E-01
C_{m_α}	-1.61352E+00	-1.34461E+00	-1.33607E+00	-1.19597E+00	-1.53106E+00
C_{m_p}	-1.57721E-03	1.72766E-01	2.08004E-01	2.36287E-01	2.78869E-02
C_{m_q}	-1.21637E+01	-1.17359E+01	-1.15910E+01	-1.14989E+01	-1.19522E+01
$C_{m_{\delta_a}}$	8.88345E-04	3.36563E-02	-4.79343E-02	-1.08155E-01	-1.05554E-01
$C_{m_{\delta_s}}$	1.72049E+00	1.71600E+00	1.71501E+00	1.71362E+00	1.71907E+00
C_{l_α}	-8.83598E-04	1.46705E-01	2.22338E-01	3.12660E-01	4.09210E-02
C_{l_β}	-8.17213E-02	-8.00520E-02	-7.91327E-02	-7.96816E-02	-8.24464E-02
C_{l_p}	-4.04776E-01	-3.11563E-01	-2.77903E-01	-2.50060E-01	-3.90565E-01
C_{l_q}	1.81228E-03	2.17391E-01	3.35373E-01	4.81226E-01	1.18673E-01
C_{l_r}	1.02180E-01	9.95691E-02	9.88831E-01	9.95305E-02	1.03046E-01
$C_{l_{\delta_a}}$	1.19518E-01	1.26233E-01	9.97864E-02	6.44079E-02	6.37744E-02
$C_{l_{\delta_s}}$	-8.90671E-04	-3.17915E-03	-4.31597E-03	-5.58684E-03	-1.79059E-03
$C_{l_{\delta_r}}$	5.03190E-02	4.88097E-02	4.85593E-02	4.87702E-02	5.06289E-02
C_{y_β}	-4.16945E-01	-4.17343E-01	-4.17637E-01	-4.18009E-01	-4.17038E-01
C_{y_p}	-1.06883E-01	-1.15842E-01	-1.20564E-01	-1.27375E-01	-1.09686E-01
$C_{y_{\delta_r}}$	2.16641E-01	2.16942E-01	2.17074E-01	2.17316E-01	2.16715E-01
C_{n_α}	-2.66125E-04	4.95746E-03	9.94213E-03	1.62459E-02	2.42717E-03
C_{n_β}	2.02555E-01	2.02757E-01	2.02899E-01	2.03094E-01	2.02597E-01
C_{n_p}	5.41511E-02	5.83790E-02	6.06617E-02	6.35370E-02	5.54097E-02
C_{n_q}	3.12841E-04	7.39130E-03	1.57035E-02	2.60384E-02	7.94506E-03
C_{n_r}	-2.64187E-01	-2.64472E-01	-2.64621E-01	-2.64867E-01	-2.64243E-01
$C_{n_{\delta_a}}$	7.57369E-03	7.64696E-03	6.27860E-03	3.67670E-03	3.78637E-03
$C_{n_{\delta_s}}$	-2.66566E-04	-3.73617E-04	-4.72809E-04	-6.23436E-04	-3.49212E-04
$C_{n_{\delta_r}}$	-1.29370E-01	-1.29519E-01	-1.29585E-01	-1.29709E-01	-1.29403E-01

Table 7. Aerodynamic Coefficient Derivatives at Mach 0.7

Mach = 0.7					
Model	Baseline	Damage 1	Damage 2	Damage 3	Damage 4
C_{z_α}	5.15479E+00	4.58625E+00	4.25004E+00	3.50202E+00	4.87709E+00
C_{z_q}	-1.11120E+01	-1.03106E+01	-9.84836E+00	-8.46320E+00	-1.02645E+01
$C_{z_{\delta_a}}$	-2.22216E-04	4.29017E-02	-8.71711E-02	-3.46944E-01	-3.49901E-01
$C_{z_{\delta_s}}$	7.49472E-01	7.39272E-01	7.33980E-01	7.18922E-01	7.40505E-01
C_{m_α}	-1.98009E+00	-1.62726E+00	-1.46588E+00	-9.14994E-01	-1.73563E+00
C_{m_p}	3.25451E-04	2.11031E-01	3.03260E-01	4.42684E-01	8.89820E-02
C_{m_q}	-9.76679E+00	-9.23551E+00	-9.01596E+00	-7.92257E+00	-8.97036E+00
$C_{m_{\delta_a}}$	-6.28767E-04	4.31118E-02	-5.31139E-02	-2.98399E-01	-3.03681E-01
$C_{m_{\delta_s}}$	1.31379E+00	1.30749E+00	1.30510E+00	1.29420E+00	1.30552E+00
C_{l_α}	1.07583E-03	1.76055E-01	2.58507E-01	4.06247E-01	5.98702E-02
C_{l_β}	-9.61119E-02	-9.21453E-02	-9.15835E-02	-9.28137E-02	-9.68908E-02
C_{l_p}	-4.49736E-01	-3.42647E-01	-3.03799E-01	-2.65389E-01	-4.30996E-01
C_{l_q}	-1.89509E-04	2.46285E-01	3.63092E-01	6.04267E-01	1.70703E-01
C_{l_r}	1.23854E-01	1.18732E-01	1.17994E-01	1.19517E-01	1.24789E-01
$C_{l_{\delta_a}}$	1.39481E-01	1.49958E-01	1.18647E-01	7.38329E-02	7.15809E-02
$C_{l_{\delta_s}}$	5.40273E-04	-2.22091E-03	-3.36939E-03	-5.52093E-03	-9.88611E-03
$C_{l_{\delta_r}}$	6.15065E-02	5.89076E-02	5.84919E-02	5.90831E-02	6.18118E-02
C_{y_β}	-4.17418E-01	-4.18123E-01	-4.18441E-01	-4.18878E-01	-4.17640E-01
C_{y_p}	-1.02890E-01	-1.13041E-01	-1.19166E-01	-1.29941E-01	-1.07278E-01
$C_{y_{\delta_r}}$	2.22029E-01	2.22479E-01	2.22683E-01	2.22993E-01	2.22203E-01
C_{n_α}	2.23320E-04	7.73506E-03	1.26650E-02	3.07653E-02	5.67604E-03
C_{n_β}	2.01431E-01	2.01765E-01	2.01919E-01	2.02116E-01	2.01542E-01
C_{n_p}	5.16275E-02	5.65227E-02	5.95166E-02	6.51267E-02	5.38698E-02
C_{n_q}	-1.71128E-04	1.06530E-02	1.71238E-02	4.71075E-02	1.73886E-02
C_{n_r}	-2.63816E-01	-2.64247E-01	-2.64445E-01	-2.64706E-01	-2.63965E-01
$C_{n_{\delta_a}}$	1.39791E-02	1.47233E-02	1.26119E-02	7.06278E-03	7.04896E-03
$C_{n_{\delta_s}}$	1.05204E-04	-4.66810E-04	-1.30435E-04	-4.76285E-04	-9.26175E-05
$C_{n_{\delta_r}}$	-1.33899E-01	-1.34113E-01	-1.34211E-01	-1.34354E-01	-1.33987E-01

Table 8. Dynamic Pressure Variables - Standard Sea Level

	Mach Number			
	0.4	0.5	0.6	0.7
Dynamic Pressure, psi	1.7811	2.7821	4.0075	5.4571

Table 9. Comparison of Aeroelastic Effects for Baseline and Damaged Wings

Mach = 0.7					
Model	Baseline	Damage 1	Damage 2	Damage 3	Damage 4
Damage Percentage	0.0 %	8.0 %	13.73 %	30.3 %	6.63 %
Total Wing Area, in^2	24319.1	23353.44	22649.67	20634.76	23513.48
Maximum Deflection, in	4.5168	3.5429	3.1171	2.3947	4.2697
Lift coefficient	0.8992	0.8001	0.7414	0.6109	0.8508
Total Lift, lb	119,334.4	101,966.4	91,638.2	68,790.9	109,170.8
Angle of Attack, deg	10	10	10	10	10
Rolling Moment Coefficient	0.000187	0.030712	0.045096	0.070868	0.010444

Table 10. Trim Values at Level Flight at Mach 0.7

Trim at Level Flight at Mach 0.7					
	Baseline	Damage 1	Damage 2	Damage 3	Damage 4
δ_a, rad	0.0	0.0	0.0	0.0	0.0
δ_e, rad	8.05331E-05	7.04628E-05	6.35912E-05	1.26446E-05	7.31528E-05
δ_r,rad	0.0	0.0	0.0	0.0	0.0
α, rad	5.60787E-05	6.35118E-05	7.24653E-05	1.16160E-04	5.79581E-05
β, rad	1.66542E-06	7.37742E-07	-2.70060E-06	1.89746E-05	3.44328E-06
p, rad/sec	2.44259E-07	3.37317E-05	6.53781E-05	2.00482E-04	8.04404E-06
q, rad/sec	0.0	0.0	0.0	0.0	0.0
r, rad/sec	1.40055E-06	9.53687E-05	1.59679E-05	7.71279E-05	5.46505E-06

Table 11. c.g. Change for Stick-Free at Mach 0.7

Model	c.g. Location	C_{m_α}	C_{m_q}	Total Weight of Aircraft, lb
Baseline	1.2838	-1.98009	-9.76679	11496.67
Damage 1	1.0725	-1.62726	-9.23551	11451.44
Damage 2	0.9553	-1.46588	-9.01596	11424.57
Damage 3	0.6188	-0.91499	-7.92257	11336.81
Damage 4	1.0700	-1.73563	-8.97036	11458.93

NOTE : c.g. = $X_{c.g.}/\bar{c}$

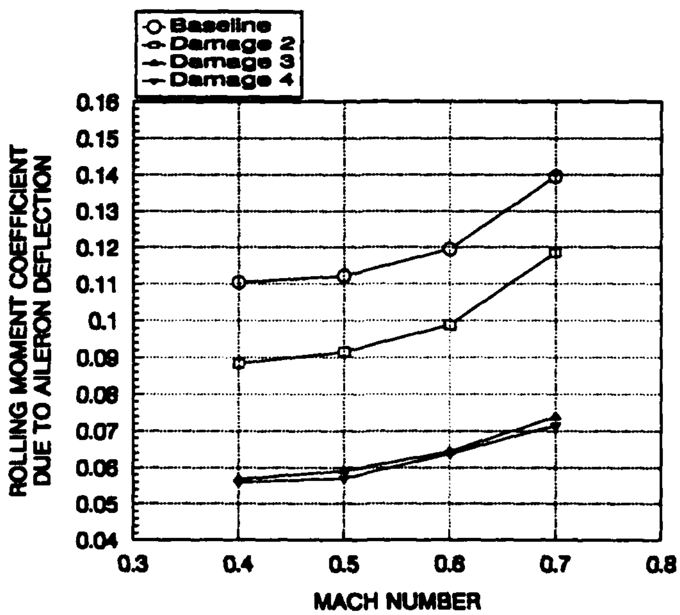

Figure 7. $C_{l_{\delta_a}}$ vs Mach = 0.4, 0.5, 0.6, and 0.7.

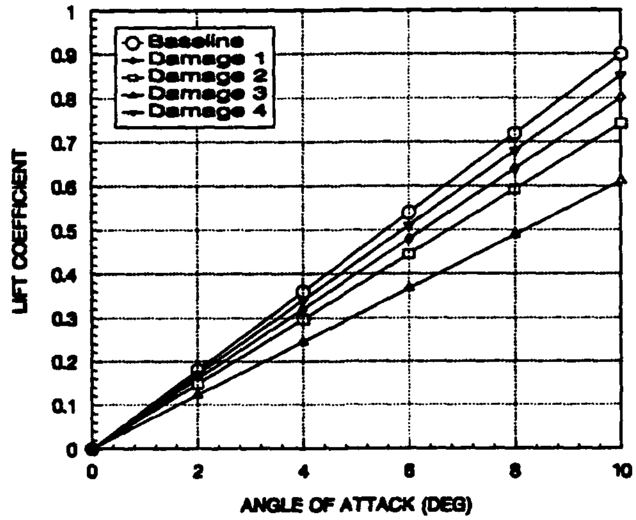

Figure 8. Lift coefficient at Mach=0.7, α=0°, 2.0°, 4.0°, 6.0°, 8.0°, and 10.0°.

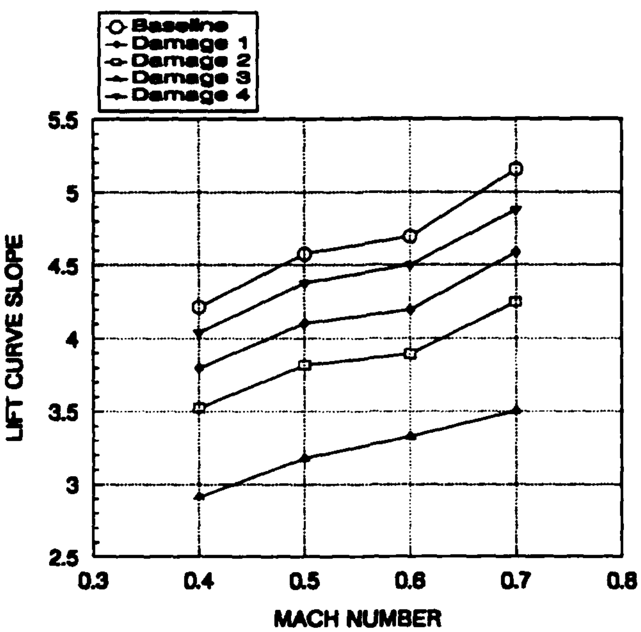

Figure 9. Lift curve slope vs Mach=0.4, 0.5, 0.6, and 0.7.

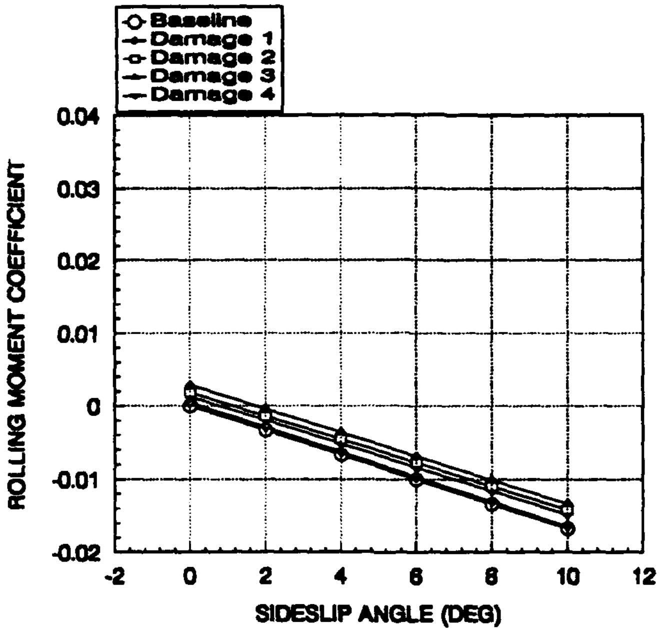

Figure 10a. Rolling moment coefficient at Mach=0.7, α=0.4°.

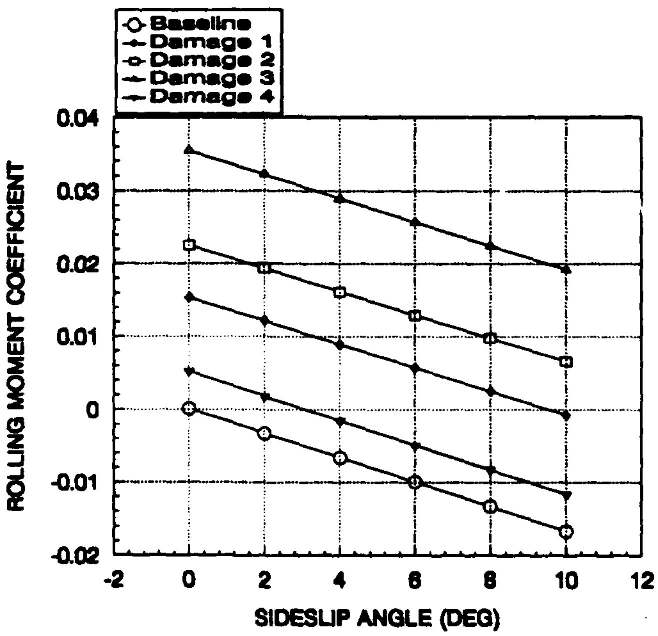

Figure 10b. Rolling moment coefficient at Mach=0.7, α=5.0°.

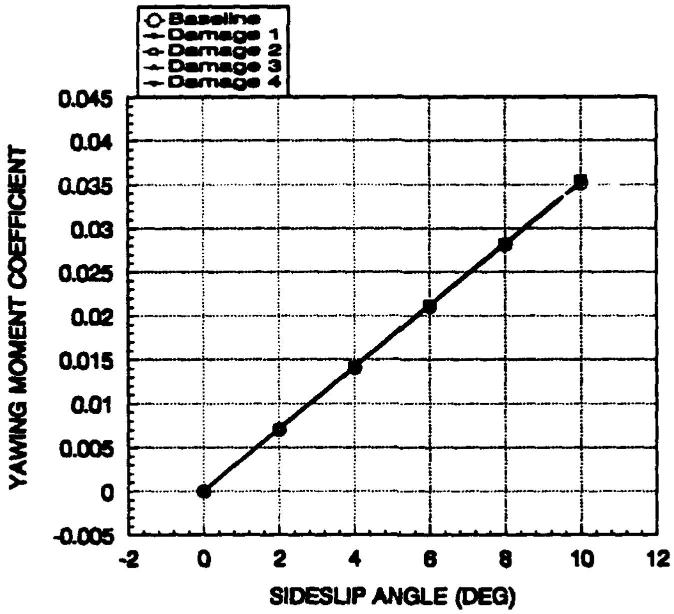

Figure 11a. Yawing moment coefficient at Mach=0.7, α=0.4°.

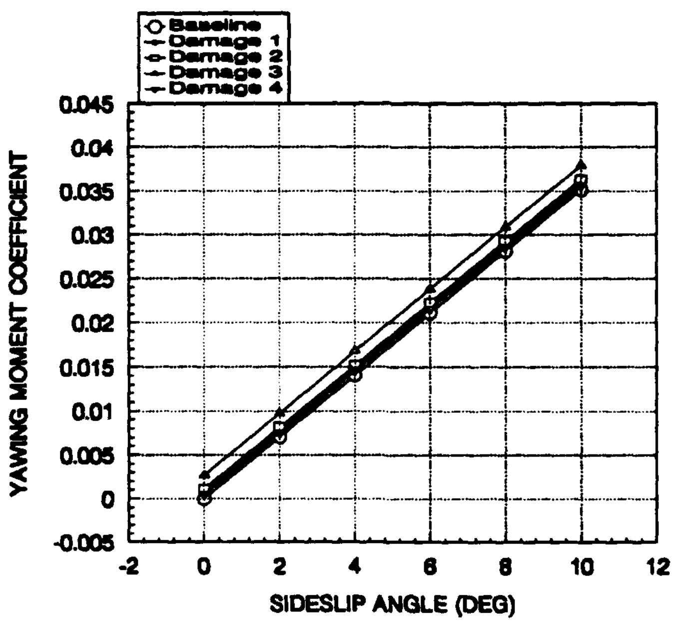

Figure 11b. Yawing moment coefficient at Mach=0.7, α=5.0°.

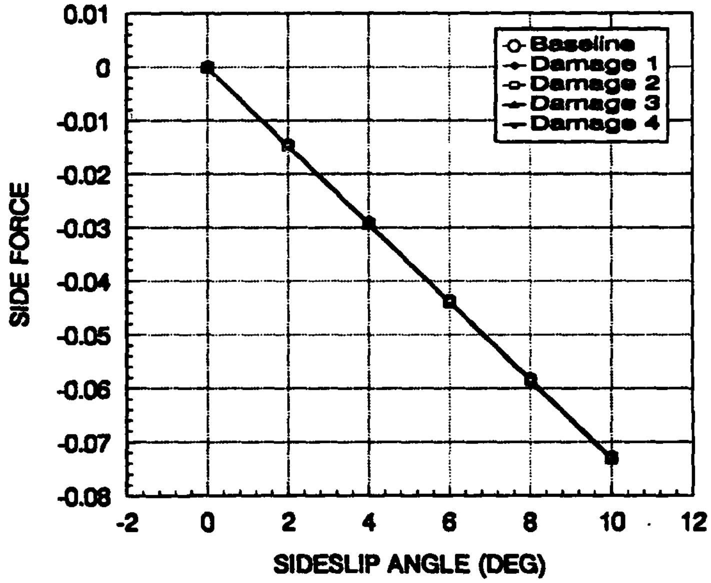

Figure 12a. Side force coefficient at Mach=0.7, α=0.4°.

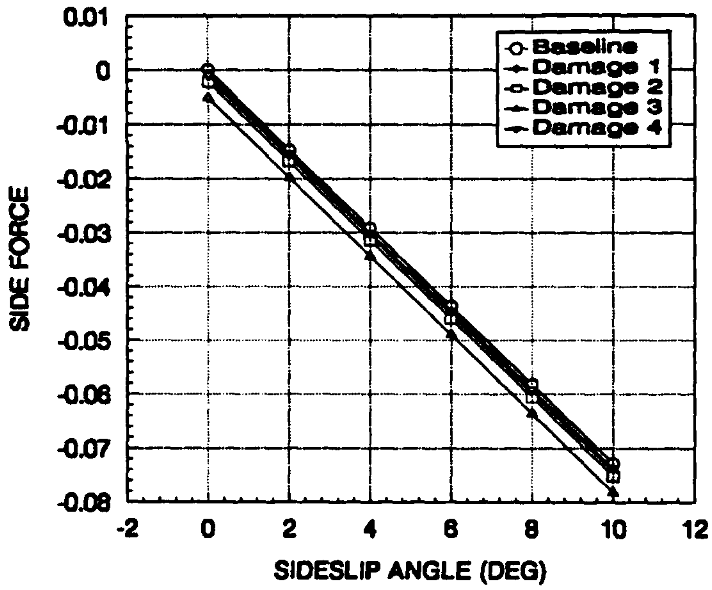

Figure 12b. Side force coefficient at Mach=0.7, α=5.0°.

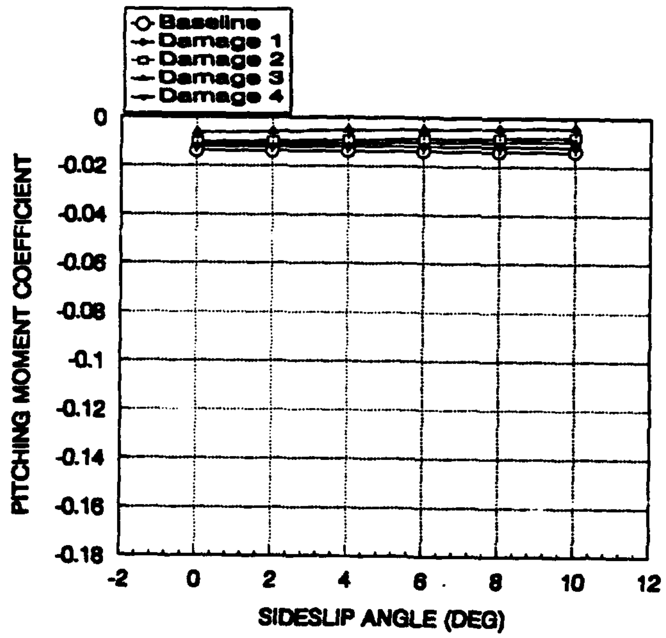

Figure 13a. Pitching moment coefficient at Mach=0.7, α=0.4°.

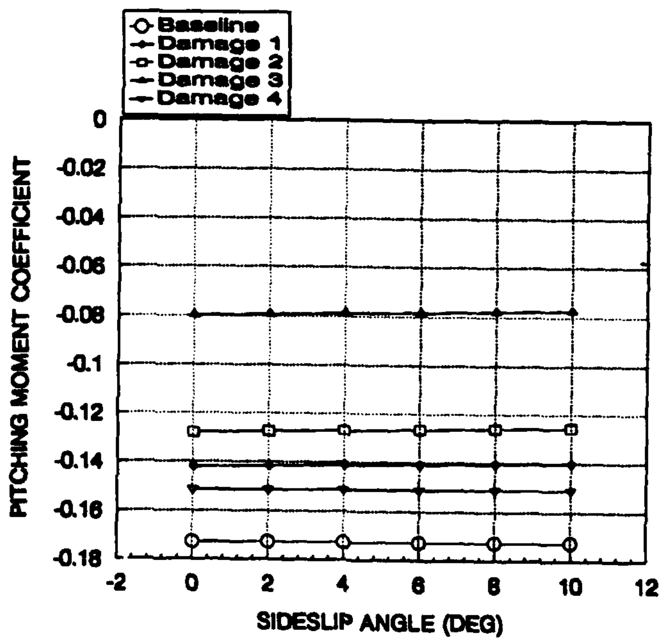

Figure 13b. Pitching moment coefficient at Mach=0.7, α=5.0°.

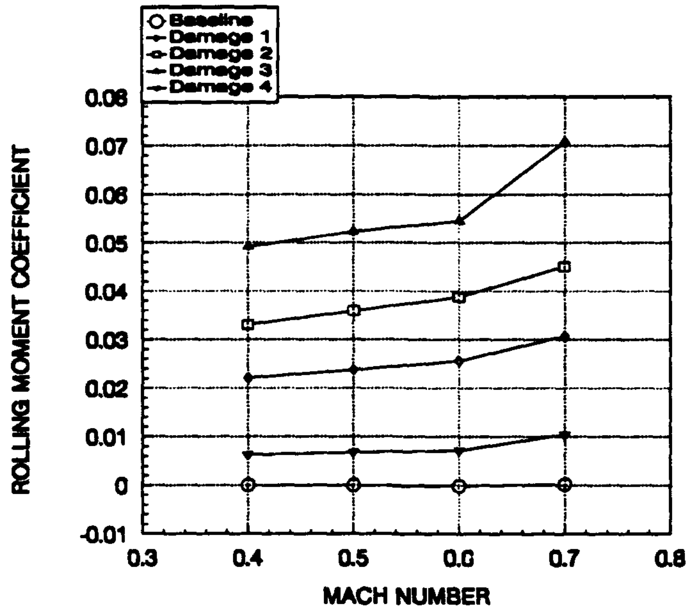

Figure 14. Rolling moment coefficient vs Mach=0.4, 0.5, 0.6, and 0.7, α=10.0°.

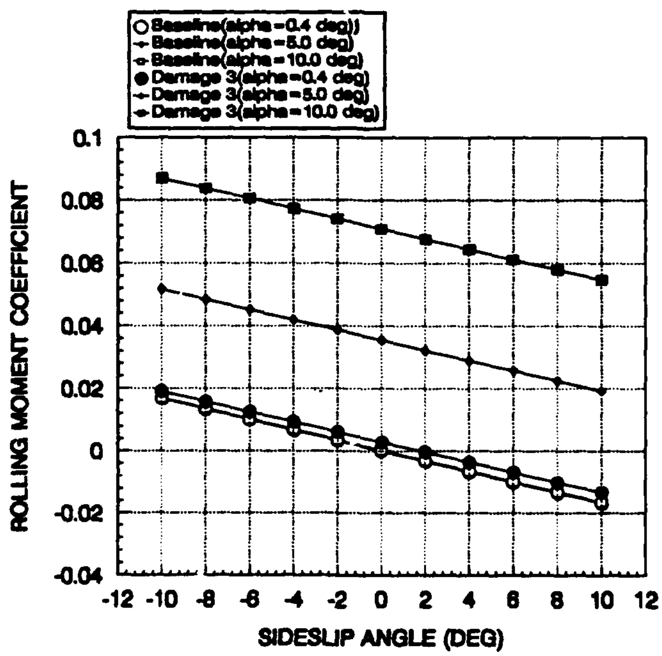

Figure 15. Rolling moment coefficient vs sideslip at Mach=0.7, α=0.4°, 5.0°, and 10.0°.

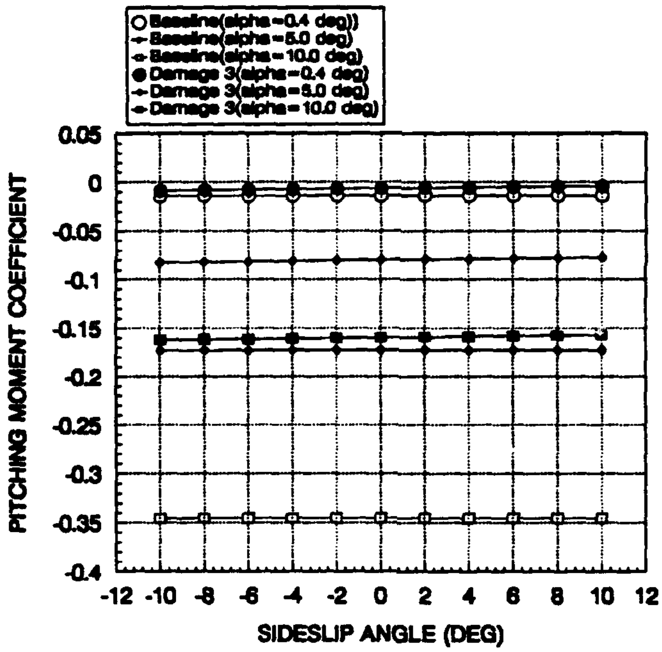

Figure 16. Pitching moment coefficient vs sideslip at Mach=0.7, α=0.4°, 5.0°, and 10.0°.

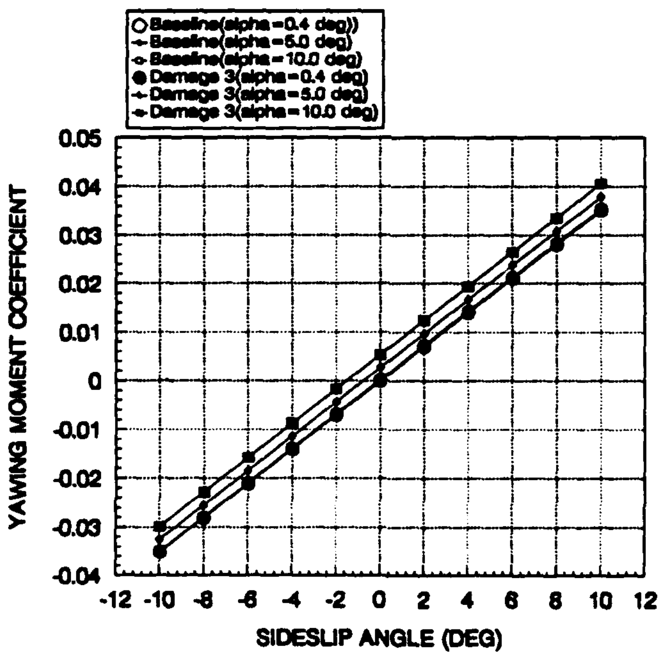

Figure 17. Yawing moment coefficient vs sideslip at Mach=0.7, α=0.4°, 5.0°, and 10.0°.

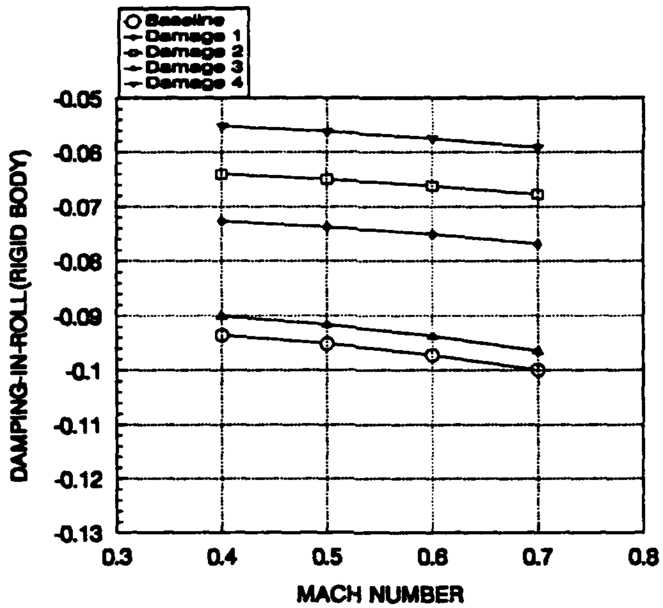

Figure 18a. Damping-in-roll elastic wing.

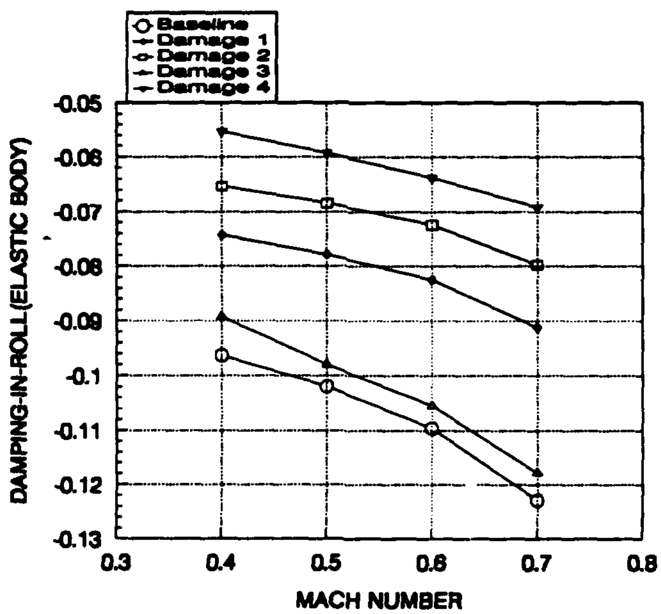

Figure 18b. Damping-in-roll rigid wing.

7. CONCLUSIONS

This study analyzed the static aeroelastic response of an aircraft with asymmetric wing planforms representative of combat damage. Trim variables, static deformations, air loads, and the aerodynamic coefficients and derivatives are obtained for both undamaged and damaged wing cases.

The following conclusions are drawn from this study.

1) The effect of longitudinal/lateral coupling for an asymmetric wing configuration is quite significant with wing damage.

2) The rolling moment coefficient is the most important stability derivative in the study of aircraft with wing damage. As discussed above, the effects are significantly influenced by the angle of attack.

3) Based on trim considerations, possible flight attitudes (angle of attack and sideslip) were found that will permit straight and level flight for a contemporary aircraft configuration with a major loss of the aerodynamic lifting and control surfaces. However, unstable dynamic modes may exist which could render the aircraft difficult or impossible to control. To address this possibility, the present results will be used with an aircraft simulation code (ACSIM) based on a coupled six degree-of-freedom aircraft equation of motion analysis.

Wing-body-tail interference effects are being considered for future study to predict the aerodynamic effects of combined damage configurations, i.e., fuselage damage combined with a damaged wing, a damaged stabilator, and/or a damaged vertical tail.

8. RECOMMENDATIONS

Through this research, three recommendations for future study are suggested. a) Investigate the effects of the aeroelastic response of a damaged stabilator or vertical wing, and develop a structural and aerodynamic model of the tail group. b) Based on the author's experience with finite element wing models (See [5] and [6]), the box-beam type wing model should be optimized as a plate-beam type wing model to save computing time and to make it easier to build a finite element model for damaged wing cases for static aeroelastic, flutter, and dynamic response analysis using the MSC/NASTRAN aeroelastic solution. c) A wind tunnel test should be planned and conducted to develop criteria to correlate the calculation method of the damaged wing aerodynamics.

INTENTIONALLY LEFT BLANK

9. REFERENCES

[1] Woo, Jong-Ho. "Static Aeroelastic Analysis of a Maneuvering Aircraft with Damaged Wing." Proceedings of the Fourth AIAA/USAF/NASA/OAI Symposium on Multidisciplinary Analysis and Optimization, Cleveland, OH, 21-23 September 1992.

[2] Albano, E., and W. P. Rodden. "A Doublet-Lattice Method for Calculating Lift Distributions on Oscillating Surfaces in Subsonic Flows." AIAA J., vol. 7, no. 2, pp. 279-285, February 1969, and no. 11, p. 2192, November 1969.

[3] Rodden, W. P., J. P. Giesing, and T. P. Kalman. "Refinement of the Nonplanar Aspects of the Subsonic Doublet-Lattice Lifting Surface Method." Journal of Aircraft, vol. 9, no. 1, pp. 69-73, January 1972.

[4] Giesing, J. P., T. P. Kalman, and W. P. Rodden. "Subsonic Unsteady Aerodynamics for General Configurations; Part I - Direct Application of the Nonplanar Doublet-Lattice Method." Air Force Flight Dynamics Laboratory Report No. AFFDL-TR-71-5, part I, vol. I, November 1971.

[5] Woo, Jong-Ho. "Static and Dynamic Analysis of T-38 Wing." Proceedings of 12th Army Symposium on Solid Mechanics (Synergism of Mechanics, Mathematics, and Materials), 4-7 November 1991.

[6] Woo, Jong-Ho. "Analysis of the Static and Dynamic Response of a T-38 Wing and Comparison with Experimental Data." US Army Research Laboratory Technical Report, ARL-TR-99, Aberdeen Proving Ground, MD, March 1993.

[7] Giesing, J.P., T.P. Kalman, and W.P. Rodden. "Subsonic Unsteady Aerodynamics for General Configurations." Technical Report AFFDL-TR-71-5, part II, vol. I, April 1972.

[8] Harder, R.L., and R.N. Desmarais. "Interpolation Using Surface Splines." Journal of Aircraft, vol. 9, no. 2, pp.189-191, February 1972.

[9] MSC/NASTRAN Handbook for Aeroelastic Analysis, vol. 1-2. The Macneal-Schwendler Corporation, November 1987.

INTENTIONALLY LEFT BLANK

10. BIBLIOGRAPHY

[1] NOR-60-6. Static Test of Complete Airframe for the T-38A Airplane. Hawthorne, California: Northrop Aircraft, Inc., March 1960.

[2] Perkins, D. Courtland., and E. Robert Hage. Airplane Performance Stability and Control. John Wiley & Sons, Inc., 1958.

[3] Bisplinghoff, R. L., H. Ashley, and R. L. Halfman. Aeroelasticity. Addison-Wesley Publishing Co., 1955.

[4] MSC/NASTRAN Aeroelastic Supplement. The Macneal-Schwendler Corporation, October 1984.

[5] Nicolai, L. Leland. Fundamentals of Aircraft Design. Doicone: Printing Services., 1975.

[6] Etkin, Bernard. Dynamics of Atmospheric Flight. John Wiley & Sons, Inc., 1972.

[7] Hurt, H. H. Aerodynamic for Naval Aviators. U.S. Navy, 1960.

[8] Stronge, W.J. "Failure Prediction for Damaged Aircraft Wings." Proceedings of the Fifth Navy-NASTRAN Colloquium, NSRDC, 1974.

[9] Liu, D.D., D.K. James, P.C. Chen, and A.S. Pototsky. "Flutter Studies of Harmonic Gradient Method for Supersonic Aeroelastic Applications." Paper 89-068, DGLR/AAAF/RAES European Forum on Aeroelasticity and Structural Dynamics, Aachen, West Germany, 17-19 April 1989.

[10] Chen, P.C., and D.D.Liu. "A Harmonic Gradient Method for Unsteady Supersonic Flow Calculations." Journal of Aircraft, vol. 22, no. 5, pp. 371-379, May 1985.

INTENTIONALLY LEFT BLANK

APPENDIX A:

Data Input and Generation for MSC/NASTRAN Aeroelasticity

INTENTIONALLY LEFT BLANK

A1. Data Input and Generation

Aerodynamic calculations are performed using a Cartesian coordinate system. By user convention, the flow is in the positive x-direction and x-axis of every aerodynamic element and must be parallel to the flow in its undeformed position. The basic structural coordinate system may be defined independently, since the use of the same system for both would place an undesirable restriction upon the description of the structural model; and any MSC/NASTRAN Cartesian system may be specified, as long as the flow is defined in the direction of the x-axis. All aerodynamic element and grid point data, initially defined in the basic coordinate system, will be transformed to the aerodynamic coordinate system. All the global (displacement) coordinate systems of the aerodynamic grid points will have their x-directions in the flow direction. Their z-directions will be normal to the element in the case of boxes, and parallel to the aerodynamic z-direction in the case of bodies.

The aerodynamic grid points are physically located at the center of the boxes for the lifting surface theories, and at the centers of body elements for the Doublet-Lattice method. Permanent constraints are generated for the unused degrees of freedom. A second set of grid points is used only for the element identification number. For any panel, the box numbers start with the panel identification number and increase consecutively.

A2. Aerodynamic Modeling in MSC/NASTRAN

Based on the guidelines explained above in section A1, the descriptions of input data to create the aerodynamic model are shown in card format in Tables A1-A3. These all option cards are used in the BULK DATA CARD [Ref. 9].

Table A1. Aerodynamic Elements

Bulk Data Entry	Description
AEFACT	Specifies lists of real numbers for aeroelastic analysis
AELINK	Defines relationship between AESTAT and AESURF entries

AELIST	Defines a list of aerodynamic elements to undergo the motion prescribed with the AESURF Bulk Data entry for static aeroelasticity
AESTAT	Specifies rigid body motions to be used as trim variables in static aeroelasticity
AESURF	Specifies an aerodynamic control surface
CAERO1	Defines an aerodynamic macro element (panel) in terms of two leading edge locations and side chords. This is used for Doublet-Lattice theory for subsonic aerodynamics
CAERO2	Defines aerodynamic slender body and interface elements for Doublet-Lattice aerodynamics
PAERO1	Defines aerodynamic panel properties in the Doublet-Lattice method
PAERO2	Defines the cross-sectional properties of aerodynamic bodies
AEROS	Basic physical data for static aeroelasticity

Table A2. Aeroelastic Response Analysis

Bulk Data Entry	Description
TRIM	Specifies constraints for aeroelastic trim variables

Table A3. Aerodynamic to Structure Interconnection

Bulk Data Entry	Description
SET1	Defines a set of structural grid points by a list
SPLINE1	Defines a surface spline for interpolating out-of-plane motion for aeroelastic problems
SPLINE2	Defines a beam spline for interpolating panels and bodies for aeroelastic problems

APPENDIX B:

Description of Aerodynamic Model

INTENTIONALLY LEFT BLANK

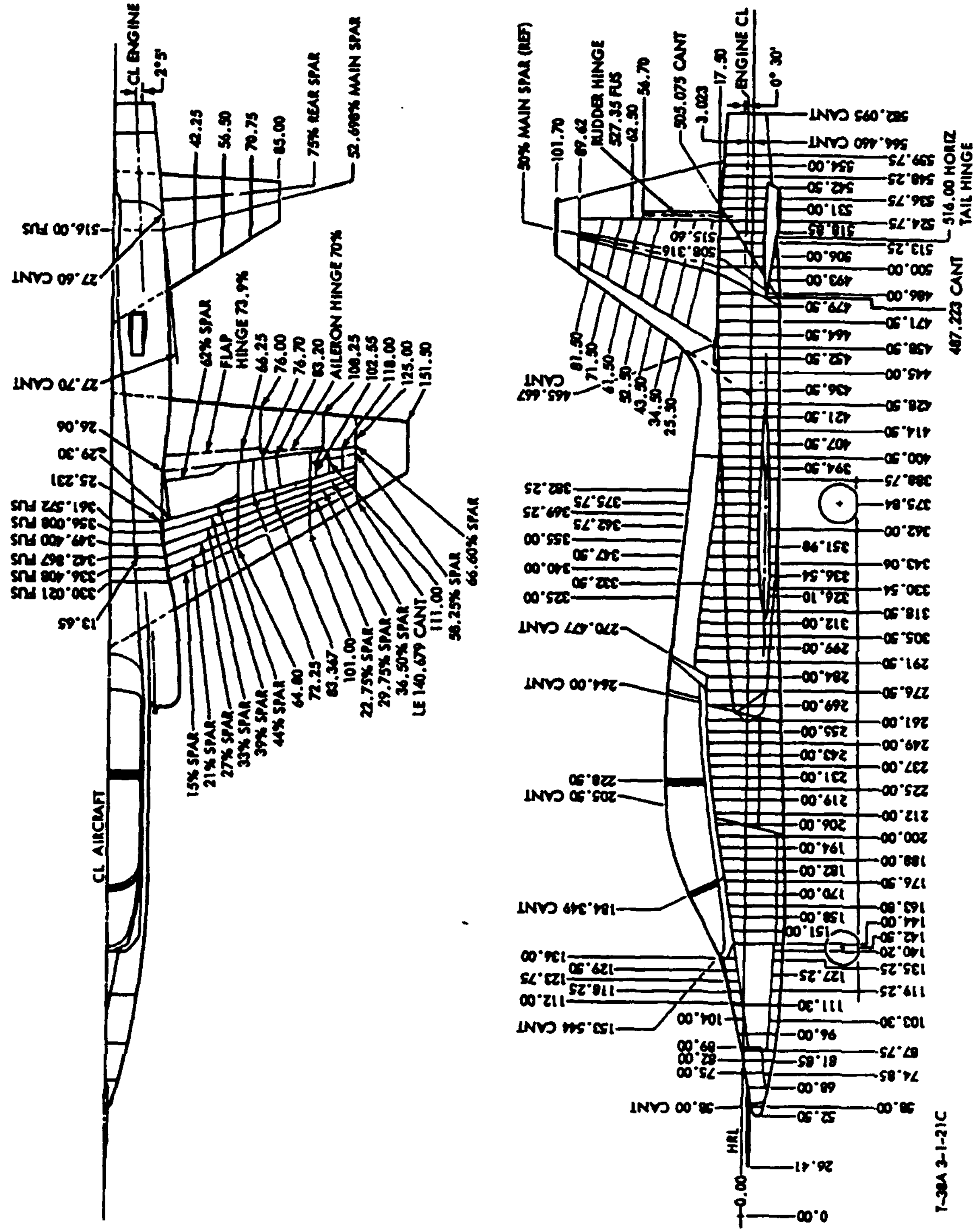

Figure B1. Structural stations of the T-38 aircraft, topview and sideview.

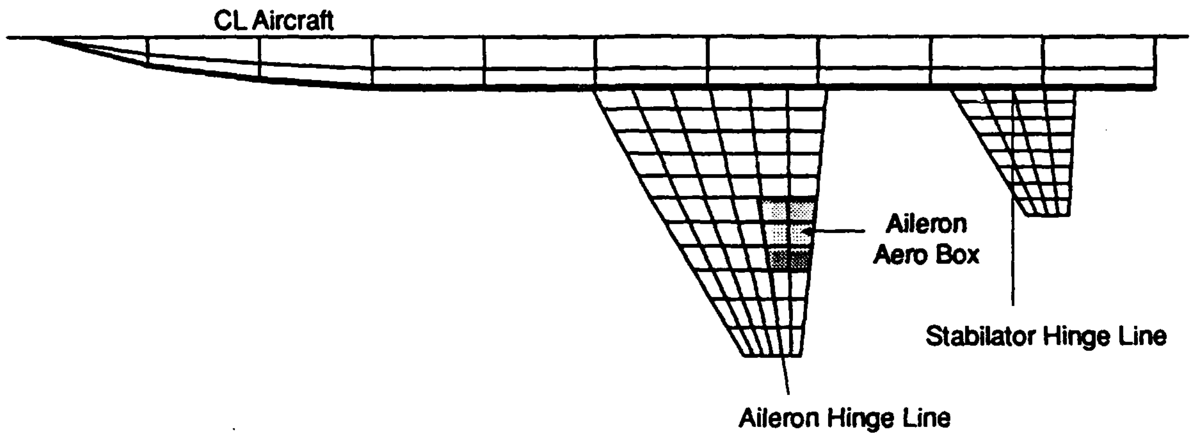

NOTE: The stabilator is an all moving tail

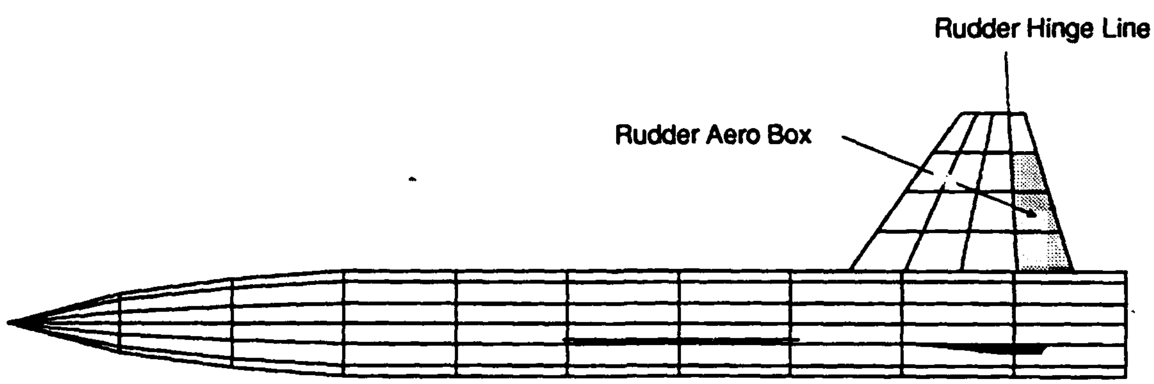

Figure B2. Hinge lines for control surfaces.

APPENDIX C:

Solution Process for Static Aeroelastic Analysis in MSC/NASTRAN

INTENTIONALLY LEFT BLANK

C1. Introduction

As described earlier in this report, the static aeroelastic analysis is designed to obtain both structural and aerodynamic data. The structural data of interest include loads, deflections, and stresses. The aerodynamic data include stability and control derivatives and trim values. The analysis presupposes a structural model, an aerodynamic model, and the interpolation between the two. In this report, MSC/NASTRAN V67 on the all Cray computer is used to analyze this study using Sol 21 or 144 (for super-element) on the Executive Control Card Deck.

C2. Option for the Case Control Card

The static deflections, stress, strain, loads, aerodynamic pressures, and aerodynamic forces are obtained as part of the options shown in Table C1. These derived quantities of interest must all be requested in the Case Control Deck. The various flight conditions are specified for each SUBCASE on TRIM cards.

Table C1. Option Card for Output

Card	Description of Output
APRES	Request the aerodynamic pressures
AEROF	Request the aerodynamic forces
FORCE	Request the structural elements loads
DISP	Request the structural deflections
STRESS	Request the structural element stresses

C3. Option for the Bulk Data Card

In the Bulk Data Card Deck, PARAM POST is used to create an external database that can be used for plotting. The POST = 0 option is for MSC/XL. The database can be used to plot analysis results; for example, to generate contour plots of stress, strain, and displacements on an aircraft wing due to airloading.

The stability derivatives are obtained as part of the solution process and are always printed as follows request. These are shown in Table C2.

Table C2. Option Card for Stability Derivatives

Label	Description
ANGLEA	Angle of attack
SIDES	Angle of sideslip
PITCH	Pitch rate
ROLL	Roll rate
YAW	Yaw rate
AILERON	Deflection of aileron
ELEV	Deflection of elevator
RUDDER	Deflection of rudder
URDD2	Lateral acceleration
URDD3	Vertical acceleration
URDD4	Roll acceleration
URDD5	Pitch acceleration
URDD6	Yaw acceleration

No. of Copies	Organization
2	Administrator Defense Technical Info Center ATTN: DTIC-DDA Cameron Station Alexandria, VA 22304-6145
1	Commander U.S. Army Materiel Command ATTN: AMCAM 5001 Eisenhower Ave. Alexandria, VA 22333-0001
1	Director U.S. Army Research Laboratory ATTN: AMSRL-OP-CI-AD, Tech Publishing 2800 Powder Mill Rd. Adelphi, MD 20783-1145
1	Director U.S. Army Research Laboratory ATTN: AMSRL-OP-CI-AD, Records Management 2800 Powder Mill Rd. Adelphi, MD 20783-1145
2	Commander U.S. Army Armament Research, Development, and Engineering Center ATTN: SMCAR-IMI-I Picatinny Arsenal, NJ 07806-5000
2	Commander U.S. Army Armament Research, Development, and Engineering Center ATTN: SMCAR-TDC Picatinny Arsenal, NJ 07806-5000
1	Director Benet Weapons Laboratory U.S. Army Armament Research, Development, and Engineering Center ATTN: SMCAR-CCB-TL Watervliet, NY 12189-4050
(Unclass. only)1	Commander U.S. Army Rock Island Arsenal ATTN: SMCRI-IMC-RT/Technical Library Rock Island, IL 61299-5000
1	Director U.S. Army Aviation Research and Technology Activity ATTN: SAVRT-R (Library) M/S 219-3 Ames Research Center Moffett Field, CA 94035-1000

No. of Copies	Organization
1	Commander U.S. Army Missile Command ATTN: AMSMI-RD-CS-R (DOC) Redstone Arsenal, AL 35898-5010
1	Commander U.S. Army Tank-Automotive Command ATTN: ASQNC-TAC-DIT (Technical Information Center) Warren, MI 48397-5000
1	Director U.S. Army TRADOC Analysis Command ATTN: ATRC-WSR White Sands Missile Range, NM 88002-55
1	Commandant U.S. Army Field Artillery School ATTN: ATSF-CSI Ft. Sill, OK 73503-5000
(Class. only)1	Commandant U.S. Army Infantry School ATTN: ATSH-CD (Security Mgr.) Fort Benning, GA 31905-5660
(Unclass. only)1	Commandant U.S. Army Infantry School ATTN: ATSH-CD-CSO-OR Fort Benning, GA 31905-5660
1	WL/MNOI Eglin AFB, FL 32542-5000
	Aberdeen Proving Ground
2	Dir, USAMSAA ATTN: AMXSY-D AMXSY-MP, H. Cohen
1	Cdr, USATECOM ATTN: AMSTE-TC
1	Dir, ERDEC ATTN: SCBRD-RT
1	Cdr, CBDA ATTN: AMSCB-CI
1	Dir, USARL ATTN: AMSRL-SL-I
10	Dir, USARL ATTN: AMSRL-OP-CI-B (Tech Lib)

No. of Copies	Organization
1	Department of Army U.S. Army Natick Research Development and Engineering Center ATTN: STRNC-UE, Andreas M. Blanas Natick, MA 01760-5017
1	WL/FIBRA ATTN: Christopher E. White Bldg. 45 2130 Eighth St., Suite 11 Wright Patterson AFB, OH 45433-7552
1	WL/FIBRA ATTN: CPT Steve Pitrof Wright Patterson AFB, OH 45433-6553
1	Director U.S. Army Research Laboratory Materials Directorate ATTN: AMSRL-MA-DA, Dr. Shun-Chin Chou Watertown, MA 02172-0001
1	AFWAL/FIBA ATTN: Douglas J. Dolvin Advanced Composites A.D.P.O. Wright Patterson AFB, OH 45433-6553
1	Syracuse University Dept. of Aerospace Engineering ATTN: Prof. V. R. Murthy Syracuse, NY 13244
1	Syracuse University Dept. of Civil Engineering ATTN: Prof. James A. Mandel Syracuse, NY 13244
1	University of Notre Dame Aerospace and Mechanical Engineering ATTN: Prof. Stephen M. Batill 101 Hessert Center Notre Dame, IN 46556

No. of Copies	Organization
1	University of California, Davis Dept. of Mechanical, Aeronautical, and Materials Engineering ATTN: Prof. Nesrin Sarigul-Klijn Div. of Aeronautical Science and Engineering Davis, CA 95616
1	Southwest Research Institute ATTN: Wiede K. Cutshall Mechanical and Fluids Engineering Division 6220 Culebra Rd. San Antonio, TX 78228-0510
	Aberdeen Proving Ground
20	Director, USARL ATTN: AMSRL-SL-BA, James N. Walbert Steve Polyak Joseph Fries Ki-Chung Kim Dennis S. Lindell Jong-Ho Woo (10 copies) AMSRL-SL-I, Donald Haskell AMSRL-WT-PB, Peter Plostins AMSRL-WT-TB, Frederick Gregory Robert L. Bitting AMSRL-CI-CA, Monte Coleman

USER EVALUATION SHEET/CHANGE OF ADDRESS

This Laboratory undertakes a continuing effort to improve the quality of the reports it publishes. Your comments/answers to the items/questions below will aid us in our efforts.

1. ARL Report Number ARL-TR-153 Date of Report June 1993

2. Date Report Received ______

3. Does this report satisfy a need? (Comment on purpose, related project, or other area of interest for which the report will be used.) ______

4. Specifically, how is the report being used? (Information source, design data, procedure, source of ideas, etc.) ______

5. Has the information in this report led to any quantitative savings as far as man-hours or dollars saved, operating costs avoided, or efficiencies achieved, etc? If so, please elaborate. ______

6. General Comments. What do you think should be changed to improve future reports? (Indicate changes to organization, technical content, format, etc.) ______

CURRENT ADDRESS

Organization

Name

Street or P.O. Box No.

City, State, Zip Code

7. If indicating a Change of Address or Address Correction, please provide the Current or Correct address above and the Old or Incorrect address below.

OLD ADDRESS

Organization

Name

Street or P.O. Box No.

City, State, Zip Code

(Remove this sheet, fold as indicated, tape closed, and mail.)

(DO NOT STAPLE)

DEPARTMENT OF THE ARMY

OFFICIAL BUSINESS

BUSINESS REPLY MAIL

FIRST CLASS PERMIT No 0001, APG, MD

Postage will be paid by addressee.

NO POSTAGE
NECESSARY
IF MAILED
IN THE
UNITED STATES

Director
U.S. Army Research Laboratory
ATTN: AMSRL-OP-CI-B (Tech Lib)
Aberdeen Proving Ground, MD 21005-5066